nature portfolio

https://doi.org/10.1038/s41586-022-05679-w

Supplementary information

The carbon sink of secondary and degraded humid tropical forests

In the format provided by the authors and unedited

Supplementary information for:

The carbon sink of secondary and degraded humid tropical forests

Authors

Viola H. A. Heinrich[1,2*], Christelle Vancutsem[3,4], Ricardo Dalagnol[5,6,7], Thais M. Rosan[2], Dominic Fawcett[2], Celso H. L. Silva-Junior[6,7,8], Henrique L. G. Cassol[5,9], Frédéric Achard[10], Tommaso Jucker[11], Carlos A. Silva[12], Jo House[1], Stephen Sitch[2], Tristram C. Hales[13], Luiz E. O. C. Aragão[2,5]

Affiliations and Addresses

[1]School of Geography, University of Bristol, Bristol, UK.

[2]Faculty of Environment, Science and Economy, University of Exeter, Exeter, UK.

[3]FINCONs group, Milan, Italy

[4]Center for International Forestry Research (CIFOR), Bogor, Indonesia

[5]Earth Observation and Geoinformatics Division, National Institute for Space Research (INPE), São José dos Campos, Brazil.

[6]Institute of the Environment and Sustainability, University of California, Los Angeles - UCLA, CA 90095 USA

[7]NASA-Jet Propulsion Laboratory, California Institute of Technology, Pasadena, CA 91109, USA

[8]Programa de Pós-graduação em Biodiversidade e Conservação, Universidade Federal do Maranhão - UFMA, São Luís, MA, Brazil.

[9]School of Geosciences, University of Edinburgh, Edinburgh, UK.

[10] European Commission, Joint Research Centre, Ispra, Italy.

[11]School of Biological Sciences, University of Bristol, Bristol UK.

[12]Forest Biometrics and Remote Sensing Laboratory (Silva Lab), School of Forest, Fisheries, and Geomatics Sciences, University of Florida, Gainesville, FL, USA

[13]School of Earth and Environmental Sciences, Cardiff University, Cardiff, UK.

Corresponding author Contact:

*Email: viola.heinrich@bristol.ac.uk

This Supplementary Information includes:

- **Translations of Summary Paragraph**
- **Supplementary Note 1: Evaluation of datasets used**
- **Supplementary Note 2: Comparison of results with previous studies**
- **Supplementary Discussion 1: Exploring variability and uncertainty in our analysis**
- **Supplementary Figures**
- **Supplementary Tables**
- **Supplementary References**

Resumen (SPA): El sumidero de carbono de importancia mundial de los bosques tropicales intactos y maduros está disminuyendo debido al cambio climático, la deforestación, y la degradación provocada por la quema y tala de bosques[1–3]. Hoy en día los bosques tropicales secundarios y degradados en recuperación cubren alrededor del 10% del área de bosque tropical[4], pero la cantidad de carbono que acumulan sigue siendo incierta. En este estudio cuantificamos el sumidero de carbono sobre el suelo de los bosques en recuperación en tres regiones tropicales húmedas: la Amazonía, Borneo y África Central. Basado en productos de datos satelitales[4,5], nuestro análisis incluye los patrones heterogéneos espaciales y temporales de crecimiento en bosques secundarios y degradados, que están influenciados por factores ambientales y antropogénicos claves. En los primeros veinte años de recuperación, las tasas de crecimiento en Borneo fueron hasta 45 y 58% más altas en comparación con África Central y la Amazonía, respectivamente. Esto se debe a variables como la temperatura, el déficit hídrico y los regímenes de perturbación. Encontramos que los bosques secundarios y degradados que volvieron a crecer entre 1984-2018 acumularon 107 Tg C al año (90 a 130), compensando el 26% (21 a 34%) de las emisiones de carbono de la pérdida de bosques tropicales húmedos durante el mismo período. Por lo tanto, la protección de los bosques maduros es una prioridad. Además, estimamos que la conservación de los bosques secundarios y degradados en recuperación podria tener un potencial de sumidero de carbono factible en el futuro de 54 Tg C al año (45 a 63), en las principales regiones tropicales estudiadas.

Résume (FRA): Le puit de carbone d'importance mondiale que constituent les forêts tropicales humides intactes et anciennes est en déclin en raison du changement climatique, de la déforestation et de la dégradation due aux incendies et à l'exploitation forestière[1–3]. Les forêts tropicales humides en cours de régénération couvre désormais environ 10 % de la superficie forestière tropicale[4], mais la quantité de carbone qu'elles accumulent reste incertaine. Ici, nous quantifions le puits de carbone aérien des forêts en cours de régénération dans trois grandes régions tropicales humides ininterrompues: l'Amazonie, Bornéo et l'Afrique centrale[5,6]. Sur la base de produits dérivés de données satellitaires[4,7], notre analyse englobe les motifs spatiaux et temporels hétérogènes de croissance dans les forêts dégradées et secondaires, qui sont influencés par les principaux facteurs environnementaux et anthropiques. Au cours des vingt premières années de régénération, les taux de croissance à Bornéo étaient jusqu'à 45% et 58% plus élevés par rapport à l'Afrique centrale et à l'Amazonie, respectivement. Cela s'explique par des différences de température, déficit hydrique et régimes de perturbation. Nous constatons que les forêts dégradées et secondaires ont accumulé 107 Tg C/an (90 à 130) entre 1984 et 2018, contrebalançant 26 % (21 % à 34 %) des émissions de carbone provenant de la perte de forêts tropicales humides au cours de la même période. La protection des forêts en cours de régénération est donc une priorité. De plus, nous estimons que la conservation et la récupération des forêts dégradées et secondaires peut potentiellement constituer un futur puit de carbone de 54 Tg C/an (45 à 63) à travers les principales régions tropicales étudiées.

Abstrak (IDN): Hutan tropis lembab adalah penyerap karbon utama dunia. Namun hutan tropis lembab yang utuh dan tua telah menurun akibat perubahan iklim, deforestasi dan degradasi akibat kebakaran & penebangan[1–3]. Pemulihan hutan sekunder dan hutan terdegradasi saat ini melingkupi sekitar 10% dari area hutan tropis[4], tapi seberapa banyak karbon yang mereka akumulasikan masih tidak pasti. Dalam penelitian ini kami mengkuantifikasi penyerap karbon permukaan pada hutan yang telah pulih di tiga area lembab tropis yang utama: Amazon, Borneo dan Sentral Afrika[5,6]. Berdasarkan data satelit[4,7], analisis kami mencakup pola heterogen secara spasial dan temporal dari pertumbuhan hutan sekunder dan hutan terdegradasi, hal ini dipengaruhi oleh faktor lingkungan dan antropogenik. Pada duapuluh tahun pertama proses pemulihan, laju pertumbuhan di Borneo mencapai 45% dan 58% lebih tinggi dibandingkan Sentral Afrika dan Amazon, berturut-turut. Hal ini diakibatkan berbagai variabel seperti temperatur, defisit air dan rezim gangguan. Kami menemukan bahwa hutan sekunder dan hutan terdegradasi telah tumbuh secara terakumulasi hingga 107 Tg C yr^{-1} (90-130) antara 1984-2018, dimana hal ini menyeimbangkan balik 26% (21% - 34%) emisi karbon dari hutan tropis lembab yang hilang dalam periode yang sama. Perlindungan terhadap hutan tua haruslah menjadi prioritas. Namun, kami mengestimasi bahwa mengkonservasi hutan sekunder dan hutan terdegradasi akan menghasilkan penyerapan karbon yang berharga dimasa depan, dengan potensi 54 Tg C yr^{-1} (45-63), pada area studi utama di kawasan tropis.

Resumo (PORT): O globalmente importante sumidouro de carbono das florestas tropicais úmidas intactas está diminuindo por causa das mudanças climáticas, desmatamento e degradação causada por incêndios e exploração madeireira[1–3]. Florestas tropicais secundárias e degradadas em recuperação cobrem cerca de 10% da área de floresta tropical[4], mas o quanto de carbono elas acumulam ainda permanece incerto. Neste trabalho quantificamos o sumidouro de carbono acima do solo de florestas em recuperação em três grandes regiões tropicais úmidas contínuas: Amazônia, Bornéu e África Central[5,6]. Utilizando produtos de sensoriamento remoto[4,7], nossa análise tem como base os padrões espaciais e temporais heterogêneos de crescimento em florestas degradadas e secundárias, influenciados pelos principais fatores ambientais e antropogênicos. Nos primeiros vinte anos de recuperação, as taxas de rebrota em Bornéu chegaram a ser 45% e 58% maiores em comparação com a África Central e Amazônia, respectivamente. Isso se deve a variáveis como temperatura, déficit hídrico e regimes de perturbação. Nossos resultados demonstram que a regeneração de florestas degradadas e secundárias acumularam 107 Tg C ano^{-1} (90 a 130) entre 1984-2018, contrabalanceando cerca de 26% (21% a 34%) das emissões de carbono da perda de floresta tropical úmida durante o mesmo período. Proteger florestas intactas é, portanto, uma prioridade. Além disso, estimamos que a recuperação de florestas degradadas e secundárias pode ter um potencial de sumidouro de carbono futuro viável de 54 Tg C ano^{-1} (45 a 63), nas principais regiões tropicais estudadas.

Abstrak (MAL): Sinki karbon yang penting secara global bagi hutan lembab tropika yang utuh dan tua semakin berkurangan disebabkan oleh perubahan iklim, penebangan hutan dan degradasi daripada pembakaran dan pembalakan[1-3]. Pemulihan hutan sekunder tropika dan hutan terdegradasi kini meliputi kira-kira 10% daripada kawasan hutan tropika[4], tetapi jumlah karbon yang terkumpul masih tidak dapat dikenal pasti. Dalam kajian ini kami mengukur sinki karbon atas tanah bagi hutan yang sedang pulih merentasi tiga kawasan utama hutan berterusan lembap tropika: Amazon, Borneo dan Afrika Tengah[5,6]. Berdasarkan produk data satelit[4,7], analisis kami merangkumi corak ruang dan masa heterogen oleh pertumbuhan dalam hutan terdegradasi dan sekunder, dipengaruhi oleh pemacu utama alam sekitar dan antropogenik. Dalam tempoh dua puluh tahun pertama pemulihan, kadar pertumbuhan semula di Borneo masing-masing meningkat sehingga 45% dan 58% berbanding Afrika Tengah dan Amazon. Ini disebabkan oleh pembolehubah seperti suhu, defisit air dan rejim gangguan. Kami mendapati bahawa pertumbuhan semula hutan terdegradasi dan hutan sekunder mengumpul 107 Tg C yr^{-1} (90 hingga 130) antara 1984-2018, mengimbangi 26% (21% hingga 34%) pelepasan karbon daripada kehilangan hutan tropika lembap dalam tempoh yang sama. Oleh itu, melindungi hutan tua adalah keutamaan. Selain itu, kami menganggarkan bahawa, memulihara hutan sedang pulih yang terdegradasi dan hutan sekunder mempunyai potensi masa hadapan sebagai karbon sinki yang boleh menyerap sebanyak 54 Tg C yr^{-1} (45 hingga 63), merentasi kawasan tropika utama yang dikaji.

摘要(CHI): 由於氣候變化、森林砍伐以及火災和伐木造成的劣化，全球重要的完整、原始熱帶濕潤森林的碳匯正在減少 [1–3]。復育中的熱帶次生林和劣化森林現在覆蓋了大約 10% 的熱帶森林面積 [4]，但它們積累了多少碳仍不確定。在這個研究，我們量化了三個主要連續熱帶濕潤地區（亞馬遜、婆羅洲和中非 [5,6]）復育中森林的地上碳匯。基於衛星數據產品 [4,7]，我們的分析涵

蓋了受關鍵環境和人為驅動因素影響的劣化和次生林生長的異質空間和時間模式。在復甦的前二十年，婆羅洲的再生率分別比中非和亞馬遜高出 45% 和 58%。這是由於諸如溫度、缺水和乾擾狀態等變項。我們發現，在 1984 年至 2018 年間，重新生長的劣化和次生林積累了每年 107 Tg 碳量（90 至 130，抵消了同期潮濕熱帶森林損失造成的碳排放量的 26%（21% 至 34%）。因此，保護原始森林是當務之急。此外，我們估計在這次研究的主要熱帶地區，保護復育中的劣化和次生林具有每年 54 Tg 碳量（45 至 63）的未來可行碳匯潛力。

Astratta (ITA): La capacità delle foreste pluviali primarie nei tropici di assorbire anidride carbonica è in declino a causa dei cambiamenti climatici e del degrado di questi ecosistemi dovuto alle crescenti pressioni antropiche[1–3]. Le foreste tropicali secondarie in via di recupero oggi coprono circa il 10% delle restanti foreste tropicali[4], ma il loro contributo alla rimozione del carbonio dall'atmosfera rimane altamente incerto. In questo studio, noi stimiamo per la prima volta la quantità di carbonio rimossa dalle foreste tropicali secondarie dell'Amazonia, del Borneo e dell'Africa Centrale[5,6]. Il nostro studio si basa su stime di carbonio derivate da satelliti[4,7], e comprende l'intero spettro di foreste tropicali secondarie affette da diversi impatti antropici e che crescono in climi contrastanti. Nei primi vent'anni di recupero, il tasso di accrescimento delle foreste tropicali secondarie nel Borneo è stato più veloce di quello delle foreste dell'Africa Centrale e dell'Amazonia del 45% e 58%, rispettivamente. Questo differenze nella velocità di recupero sono legate sia a differenze di temperature e precipitazione tra queste zone, sia a differenze nella modalità ed intensità del disturbo. Complessivamente stimiamo che dal 1984-2018 le foreste tropicali secondarie hanno accumulato 107 Tg C yr^{-1} (90 to 130), controbilanciando cosi il 26% (21% to 34%) delle emissioni di carbonio causate dalla perdita di foreste tropicali pluviali avvenute nello stesso periodo. Proteggere ciò che rimane delle foreste pluviali primarie tropicali rimane quindi una priorità assoluta. Ma oltre a ciò, noi stimiamo che proteggere le foreste tropicali secondarie dell'Amazonia, Borneo e Africa Centrale risulterebbe nell'ulteriore rimozione di 54 Tg C yr^{-1} (45 to 63) dall'atmosfera.

Supplementary Notes

The Supplementary Notes provide key evaluation of the dataset used (Note 1) as well as a critical comparison of the main results achieved using these datasets in comparison with other published research, especially field data (Note 2).

Supplementary Note 1: Evaluation of datasets used

The Amazon Region – evaluation of the land-cover dataset

We compared the secondary forest classification used in this study (Joint Research Council-Tropical Moist Forest (JRC-TMF)[4] with secondary forest classification based on MapBiomas (collection 5.0)[6,7]. MapBiomas is a land-use-land cover dataset that has been used numerous times to identify secondary forest pixels in the Brazilian Amazon[8–10]. We used the code developed by Silva et al[10] to determine the extent and age of secondary forests in 2018 according to MapBiomas. As both the MapBiomas and JRC-TMF (this study[4]) datasets are Landsat derived, they have a pixel size of 30m, and overlying pixels could be directly compared (Supplementary Figure 9). We found discrepancies primarily because of differences in definitions of secondary forest. JRC-TMF[4] classified secondary forest as pixels that have remained undisturbed for at least 3 years following the initial disturbance. This limits the number of pixels compared to the MapBiomas dataset. Importantly, only a small fraction (~7%) of pixels classed as Secondary Forest in MapBiomas were classed as degraded forest in the JRC-TMF dataset, suggesting that that there are few misclassification errors of degraded and secondary forest in the JRC-TMF dataset.

We also compared the value of the pixels expressed as age (MapBiomas) or "Years since last Disturbance" (YSLD; this study) where pixels of secondary forest did overlap and found good agreement between the two datasets (r^2 = 0.61) (Supplementary Figure 10a), especially when taking the modal value (r^2 = 0.98) (Supplementary Figure 10b). This suggested that the measure YSLD, could be used as an accurate estimate for secondary forest age. Although there were discrepancies with regards to the spatial extent of secondary forest area between the two datasets, the temporal dynamics were similar, which was important for the space-for-time substitution approach used in our study.

The Amazon region – evaluation of the regrowth models

We applied the growth model for the Amazon (Figure 1 of main paper) and estimated the carbon stock in the Brazilian Amazon biome in 2018 using the JRC-TMF dataset and the MapBiomas dataset. We compared our results to previous studies conducted in the Brazilian Amazon that used other regional estimates of AGC and remote sensing data to identify secondary forest (Supplementary Table 16). We find that, the Aboveground Carbon density (the AGC per unit area) is very similar across all six of the studies. For example, the average AGC density of secondary forest was 23.7 Mg C ha^{-1} in our study, which was only 1.1 Mg C ha^{-1} lower than the study by Smith et al. (24.8 Mg ha^{-1}) which relied on the updated IPCC default values of regrowth[11] and MapBiomas to identify secondary forests[9]. However, the most noticeable difference is the area of secondary forest, which is on average 65% lower in this study compared to previous studies (Supplementary Table 16). This, therefore, makes our analysis conservative in terms of the overall carbon sink and stocks in secondary forests in the Amazon region, and potentially in the other regions too.

Borneo – evaluation of the land-cover dataset

We compared the JRC-TMF dataset in Sabah, Malaysian Borneo. Another tropical region where there has been considerable work providing spatial data on forest type and land-use-land-cover

(Supplementary Figure 11). We used a map of the types of Forest Reserves in Sabah and compared the JRC-TMF transition dataset with a previous detailed study that classified forest into different types[12]. We see differences between the dataset, especially in regions of Protected Forest Reserve, Commercial Forest Reserve and Wildlife Reserve areas. This is in part due to the differences in the method applied with regards to identifying disturbed/logged forest. Gaveau et al.[12] applied a buffer of 700 m around the roads and assumed these regions to all be logged forest areas. In contrast Vancutsem et al.[4] apply a pixel-based approach to identify disturbances, and hence the areal extent of degraded forests is lower in the JRC-TMF dataset used in this study.

Central Africa region – evaluation of the land-cover dataset

We compared the AGC of forests classed as old-growth (undisturbed) in the TMF-JRC dataset, inside and outside regions of logging concession[13] in Central Africa. We see a statistically significant lower mean AGC of old-growth forest inside (109 Mg C ha^{-1}) logging concession regions compared to outside the concessions (164 Mg C ha^{-1}) (Supplementary Figure 12). This would suggest that old-growth (undisturbed) pixels within logging concession areas experience a degree of degradation that is not detected at the scale of the JRC-TMF product[4], but which is detected by the active sensors of the AGC datasets, and therefore reflected in the total AGC of the pixel. The AGC distribution both inside and outside the concession regions is very similar, and the median value is higher inside the concession area than outside. As we relied on the median AGC value to construct our growth curves we do not believe the growth rates would be significantly affected as the median AGC of old-growth forest is unlikely to change significantly. Additionally, the effect size (0.26), which provides a measure of the magnitude of the difference between the two datasets, is small (<0.3).

Based on the degradation analysis in Borneo and the AGC analysis of old-growth forest in Central Africa it would suggest that there are likely to be more degraded forest regions than were identified in the JRC-TMF dataset[4]. This does not impact the analysis of aboveground carbon density (i.e. Mg C ha^{-1}), and therefore does not affect our estimated growth rates. However, it does mean that the total carbon stock as we have estimated it in this study is likely to be a conservative one.

Pan-tropical – evaluation of the ESA-CCI AGB/AGC dataset

Our AGC estimate for old-growth forest are about 35 to 45 Mg C ha^{-1} lower compared to field-study estimates in the three regions[14–16]. We also compared the AGC of old-growth forests obtained from the ESA-CCI Aboveground Biomass (AGB) product with the new Light Detection And Ranging (LiDAR) derived Footprint-level AGC product from the Global Ecosystem Dynamics Investigation (GEDI) mission[17–19]. We extracted the GEDI AGC data at the footprint level (~25m resolution) and resampled to 100m resolution to enable efficient processing of this large dataset (7 Tb). We then extracted all AGC pixels overlying regions of old-regrowth forest according to the JRC dataset and compared the AGC data with the ESA-CCI product (Supplementary Figure 19). We focused our analysis on old-growth forests as these represent larger areas with less forest fragmentation compared to secondary and degraded forests, limiting potential geolocation issues of the GEDI footprint product.

Across the three regions, we found the ESA and GEDI AGC estimates overlapped and were not statistically different in Central Africa ($p = 0.45$) and Borneo ($p=0.099$), where $p<0.05$ suggests that the difference in the mean value of the respective datasets is statistically significant (Supplementary Figure 19). Across the three regions, the effect size, measuring the magnitude of the difference between the datasets, was also very small (0.043 to 0.046). Overall, there was higher variability in the GEDI dataset, reflecting the higher resolution of this data and its ability to capture spatial heterogeneity. The result gives confidence in our analysis that the median AGC and associated variability is a representative measure of old-growth forest values in each region, which is an important component in the regrowth model, representing the asymptote.

The median and mean AGC estimate for old-growth forests across the three regions are similar and confidence intervals overlap (Supplementary Figure 19, Supplementary Table 2 and 4). The similarity across the three tropical regions contradicts field studies, finding old-growth forest AGC values are higher in tropical African forests than in America or South East Asia [15,20,21].

Potential hypotheses to explain why higher AGC values in Central African old-growth forests identified in field studies are neither seen in the ESA-CCI nor the GEDI datasets include: (i) the land-cover dataset (JRC-TMF) may not capture all small-scale disturbances that are common in Central Africa, however the impact of the disturbances may inherently be detected in both the AGC products compared in our analysis, thus reducing the expected AGC in old-growth forests in Central Africa; (ii) there is a systematic bias in both the ESA-CCI and GEDI dataset such that both products saturate at lower AGC values in Central Africa compared to in the Amazon and Borneo; (iii) field-based quantifications of AGC are themselves also estimates, and are limited spatially and temporally. Environmental, climatic, and anthropogenic drivers influence the spatial variability of biomass/carbon, that are still not fully understood from field-data alone, especially in under-explored regions. Continuing efforts to collect field-data in a standardised manner, especially in regions that are currently underexplored are important considerations for field explorations to ensure reference measurements on the ground are useful for remote sensing applications[22].

The second hypothesis is likely to be explored further by the Global Biomass product analysis and validation project (https://www.earthdata.nasa.gov/esds/maap). Initial results in Gabon, comparing the global products with air-borne LiDAR AGB products have shown that the ESA-CCI dataset has higher values of AGB compared to the air-borne product and begins to saturate at 300 to 400 Mg ha^{-1} (~135 to 182 Mg C ha^{-1}) [23]. Similar exercises are likely to be carried out elsewhere, providing further insight into the relative importance of the second hypothesis and third hypothesis.

Supplementary Note 2: Comparison of results with previous studies

Our study is the first of its kind to use global remote sensing products to model the recovery of degraded *and* secondary forests in terms of AGC across the tropics. The approach has the potential to capture changes occurring spatially across the three tropical regions, covering 40 years of disturbance history, something which is not possible with field data. On a local scale, field data estimates remain one of the most accurate ways to understand the tropical forest carbon dynamics. It was therefore essential to compare our results with previous studies that have relied on field data, airborne LiDAR analysis or a combination of both. Below we introduce various studies used for comparison and briefly outline the region, forest type and data type of the study, followed by a detailed assessment of the comparison that was carried out.

Overall, we found a good agreement between the previous studies and our analysis. For example, our AGC and modelled regrowth rates were not statistically different to a study in Bornean degraded forests[24]. The modelled relative recovery of AGC in Amazonian degraded forests and associated 95% confidence interval was within the modelled recovery rates of previous studies relying on either field data[25] or other remote sensing products of AGC[26,27]. Many of the comparisons where within the Amazon region and Neotropics. Access to field data in Central Africa and Borneo was more difficult given the relative sparse nature of field studies there, spatially, compared to the Neotropics. This again emphasizes the importance of being able to use remote sensing data to capture changes in forest demography and associated carbon, especially where field data is lacking. The text below provides more detail on our comparison. The corresponding Supplementary Figures and Tables appear at the end of the respective sections and are Supplementary Figures 20 to 25 and Supplementary Tables 18 to 20.

Comparison with Philipson et al (2020)[24]

- Location: Sabah, Malaysian Borneo
- Forest type: Degraded forests (by logging)
- Data type: Field data (Number of samples: 509)

Philipson et al. (2020) used field data[28] to estimate AGC recovery rates across various degraded forests by logging in Sabah as a function of the type of restoration being used. They found naturally regenerating forests recovered at a rate of 2.8 Mg C ha^{-1} yr^{-1} (CI: 2.0 to 3.6), whilst forests with active restoration recovered at a rate of 4.3 Mg C ha^{-1} yr^{-1} (CI: 3.5 to 5.0)[a]. LiDAR-derived estimates for the same region resulted in estimates of 3.4 and 4.7 Mg C ha^{-1} yr^{-1} in regions without and with active restoration, respectively.

We used the field data from Philipson et al: (i) to compare AGC field-based estimates of degraded forests (their study) with the satellite-derived estimates of AGC in degraded forests across the whole Sabah region (this study); and (ii) to apply the regrowth model used in this study on the field data and all forests identified as degraded by the JRC dataset in the Sabah region.

Our analysis found the AGC estimates based on field-data and satellite data are overall not statistically different (p-values between 0.03 and 0.4) ($p>0.01$) and that, in this relatively small region, the variability of values seen in the field data is also captured by the satellite data (Supplementary Figure 20a). A key difference was in the group 1- 5 Year Since Last Disturbance Event ($p<0.01$) where the satellite-based estimates resulted in a statistically different mean AGC value. This may in part be because in our analysis we included different types of disturbance (Supplementary Figure 21), and the field data only considered logged forests.

We also found that the modelled regrowth rate estimates and associated modelled 95% confidence interval (CI_{model}) in the first 20 years of recovery were comparable, 3.78 Mg C ha^{-1} yr^{-1} (CI_{model}: 3.63 to 3.93) and 4.47 Mg C ha^{-1} yr^{-1} (CI_{model}: 3.02 to 5.93) for the satellite-based and field-based data, respectively (Supplementary Figure 20b). Both these values in turn are similar to the estimates from the original study, which found a recovery rate between 2.8 Mg C ha^{-1} yr^{-1} (CI: 2.0 to 3.6) and 4.3 Mg C ha^{-1} yr^{-1} (CI: 3.5 to 5.0)[24].

The total amount of carbon remaining after degradation, was also similar, with overlapping confidence intervals (CI_{model}). For the field data (Philipson et al.) and satellite-based approach (our study) the AGC at 1 YSLD was 22.7 Mg C ha^{-1} (CI_{model}: 0 to 55.8 Mg C ha^{-1}) and 36.2 Mg C ha^{-1} (CI_{model}: 21.8 to 50.6 Mg C ha^{-1}), respectively. These values are equivalent to a AGC loss (or committed emission) of 143 Mg C ha^{-1} and 109 Mg C ha^{-1} compared to old-growth forest values in Sabah for the field data (166 Mg C ha^{-1}) and remote-sensing approach (131 Mg C ha^{-1}), respectively. The emission factor estimates are high compared to another study in Eastern Kalimantan on Borneo[29], where committed emissions from logging were found to be between 40 and 75 Mg C ha^{-1}. But our calculations are not outside of the modelled range provided by Philipson et al. in a linear-modelling approach. They found the AGC at 1 YSLD to be 48.5±34 Mg C ha^{-1}, equivalent to a loss (committed emission) of about 150 Mg C ha^{-1}, assuming old-growth forest AGC to be 194 Mg C ha^{-1} (146 to 243).

---

[a] These values have been adapted to reflect the AGB to AGC conversion ratio used in this study (0.456). The study originally used conversion of 0.47

Comparison with Griscom et al. (2014)[29]

- Location: East Kalimantan, Borneo
- Forest type: Degraded forests
- Data type: Field data (Number of sites: 9)

Griscom et al. analysed the AGC lost following logging activities in different types of forest certifications. They found that selective logging resulted in 46.6 Mg C ha^{-1} [b] of committed emissions, equivalent to about 20% AGC loss (based on an average 188 Mg C ha^{-1} in old-growth forests), or 80% AGC remaining after logging. Across the whole Island of Borneo, we estimated the AGC after 1 YSLD to be 13%, a stark contrast to the study by Griscom et al, although similar to the study by Philipson et al. (see earlier text).

To explore these discrepancies further, we compared AGC after degradation in logging concession areas of East Kalimantan using the AGC remote sensing product used throughout this study (ESA-CCI), with a LiDAR derived (GEDI) dataset. In this area, both remote sensing datasets suggest that the AGC after 1 YSLD is much lower (16% to 27% of old-growth forest values) compared to the field data by Griscom et al. for this region (Supplementary Figure 25).

Potential reasons for the differences between the Griscom et al. study and remote sensing products could include: (i) the remote sensing datasets are from 2018 (ESA-CCI) and 2020 (GEDI), whilst the field data analysis is from 2014, disturbance intensity may have increased in this area since the field study took place, (ii) as both remote sensing products provide higher spatial resolution compared to the field data analysis they may encompass regions of higher disturbance activity, (iii) there may be technical limitations to the remote sensing products and they both underestimate AGC in degraded forests in Borneo.

Comparison with Asner et al. (2018)[30]

- Location: Sabah, Malaysian Borneo
- Forest type: Secondary forest
- Data type: LiDAR

The study by Asner et al. (2018) used LiDAR to map the carbon stocks of different forest types. For this comparison we focus on forests regrowing from clearing (secondary forest) since 1973 (~45 years of regrowth). Although they identify other forest types there is no clear age associated with these for a suitable comparison in this study.

They find an average AGC in 45-year-old secondary forests of 76 Mg C ha^{-1} [30] [c]. Using the Borneo-wide secondary forest regrowth models developed in this study, after 45 years of regrowth we model a AGC value of 85.5 Mg C ha^{-1} (CI_{MC}: 65.4 to 112.1). The results from their study and ours are very similar with overlapping confidence intervals, suggesting that the regrowth model developed for secondary forests on Borneo representative for the region and forest type.

---

[b] These values have been adapted to reflect the AGB to AGC conversion ratio used in this study (0.456). The study originally used a conversion of 0.5

[c] This value has been adapted to reflect the AGB to AGC conversion ratio used in this study (0.456). The study originally used a conversion of 0.48

Comparison with Poorter et al. (2021)[31] ***and Cook-Patton et al. (2020)*** [32]

- Location: Neo tropics (and West Africa)
- Forest type: Secondary forests
- Data type: Field data (Number of sites: 77)

The study by Poorter et al. (2021) analysed the recovery of various attributes of secondary forests across the Neotropics and West Africa using field data[31,33]. They found that the relative recovery of Aboveground Biomass (AGB) was amongst the two slowest attributes to recover to levels equivalent to old-growth forest values, taking more than 100 years to recover to 90% AGB values of old-growth forests (see Figure 2 in Poorter et al.)[31].

We compared our model of secondary forest regrowth in the Amazon region to their results to determine whether the relative recovery (regardless of the absolute values) of the model was similar to results by Poorter et al. We also applied the mean and lowest absolute regrowth value estimated by Cook-Patton et al.[32], a linear model of regrowth for the first 30 years of secondary succession for the Amazon region. To determine the relative recovery of the model used by Cook-Patton et al. we used the mean old-growth forest value of AGC based on the refined IPCC default values for the American Tropical rainforest (140 Mg C ha^{-1})[34].

After the first 20 years of recovery, we found that AGC had recovered to 33% (Poorter et al., 2021), 66% (Cook-Patton et al., 2020) and 37% (this study) relative to old-growth forest values (Supplementary Table 18). After 30 years of recovery, these values increased to 45%, 99%, and 47% for the respective studies. Results from our study followed a similar trajectory to Poorter et al.; after 120 years, we found AGC had recovered to 85% (67% to 100%), whilst Poorter et al. estimate 90% recovery of AGC relative to old-growth forest values. The comparison suggests that the satellite-based recovery model of secondary forest for the Amazon region developed in our study provides estimates similar to field data in this region and encompass areas of slow secondary forest regrowth[35,36]. When using the lowest possible regrowth value estimated by Cook-Patton et al. for this region (2.4 Mg C ha^{-1} yr^{-1} [d]) the relative recovery is 35%, similar to the estimates by Poorter et al. and our study (Supplementary Table 18). The comparison suggests that the mean values presented by Cook-Patton et al. are likely at the upper-end of regrowth potential for this region.

Comparison with Rutishauser et al. (2015)[37]

- Location: Amazon Basin
- Forest type: Degraded forests (by logging only)
- Data type: Field data (Number of samples: 84)

Rutishauser et al. used samples across 10 locations in the Amazon basin to determine the recovery time of degraded forests following logging activities of various intensities. They found that the average recovery rate was 1.3 Mg C ha^{-1} yr^{-1} (0.04 to 2.9)[b] in all forests that recovered following the degradation event. They found logging intensity, relative to AGC values prior to logging, to be the primary indicator of recovery time. The average AGC loss was 22% of the initial values[37].

We compared our estimates of recovery in degraded forest to estimates by Rutishauser et al. and found that the average rate of recovery in the first 20 years since the last disturbance was similar to our result (1.49 Mg C ha^{-1} yr^{-1} [CI_{MC}: 1.32 to 1.65]) with overlapping confidence intervals. In our study

[d] These values have been adapted to reflect the AGB to AGC conversion ratio used in this study (0.456). The study originally used a conversion of 0.47

we found an AGC loss of 45% compared to old-growth forest values, this is higher than the 22% reduction found by Rutishauser et al. The difference may be for several reasons, firstly the study by Rutishauser et al. used field data in primarily Reduced-Impact-Logging sites with only 7.7% of the sites exposed to conventional logging, additionally none of the sites were subject to further post-logging disturbances such as fire or illegal logging, which Rutishauser et al. recognised as factors that would increase the recovery time presented by the field-based estimates. The regions identified as recovering degraded forests in our study included forests subject to various degrees of logging intensity, as well as burning (Supplementary Figure 21)[38]. Indeed, as our analysis in Supplementary Note 1 suggests, the JRC-TMF product does not capture low intensity (i.e. reduced impact logging) well. Our analysis therefore captured conventional logging and fires, which cause more damage to the forest and thus we expect our estimates to show higher AGC loss than field data analysing largely reduced impact logging. We therefore also compared our results to other studies that include a range of disturbance types (next section).

Comparison with Rappaport et al. (2018)[25] ***and Bullock and Woodcock (2021)***[26]

- Location: Mato Grosso state
- Forest type: Degraded forests (by logging and burning)
- Data type: LiDAR data and Landsat imagery

Rappaport et al. combined high-density LiDAR and Landsat data to characterise and quantify the loss of AGC after different types and intensities of disturbance as well as their recovery in the southern part of the Brazilian Amazon, in the state of Mato Grosso[25]. They found that the AGC lost after degradation was higher in regions with fire than only logging, which in turn varied by the intensity of the logging events. Overall, they found the rate of recovery was not statistically different across the different types and intensities of recovery.

We compared our model for regrowth in Amazonian degraded forests with results presented by Rappaport et al. (Table 1 and 2 of their study)[25]; looking at the AGC lost after degradation and post-disturbance recovery rates expressed as a percentage, and relative to the median AGC of old-growth (intact) forests (Supplementary Table 19).

The LiDAR-based estimates by Rappaport et al. estimated that the median AGC after 1-2 YSLD was 58.6 Mg C ha^{-1} and 62.4 Mg ha^{-1} [e] for single-burnt and logged forests, respectively[25]. We found the median AGC for 1-2 YSLD for burnt and non-burnt (logged) degraded forests to be 52.9 C Mg ha^{-1} and 77.1 Mg C ha^{-1}, respectively (Supplementary Figure 21). The multi-linear regression analysis determining AGC recovering by Rappaport et al. was compared to our non-linear model in terms of the percentage recovery in relation to old-growth/intact forests (Supplementary Table 19). Across the modelled YSLD, AGC estimates from our study were consistently between the estimates of logged and burned degraded forests by Rappaport et al. and the confidence intervals of the two studies overlapped. For example, after 10 years of recovery, the AGC of Amazonian degraded forests relative to old-growth AGC was 69.6% (CI_{MC}: 63.6% to 75.6%). According to Rappaport et al. after 10 years the relative recovery in logged and burned forests is 77.9% (CI_{MC}: 73.6% to 82.3%) and 68.9% (CI_{MC}: 63.1% to 74.7%), respectively. The results from the comparison are promising, showing that the regrowth model of degraded forest recovery in our study are similar with LiDAR derived estimates in this region of southern Amazon.

[e] These values have been adapted to reflect the AGB to AGC conversion ratio used in this study (0.456). The study originally used conversion of 0.5

Another study analysing recovery from natural disturbance and degradation in the Amazon region also compared their results to Rappaport et al. The study by Bullock and Woodcock (2021)[26] used two post-disturbance recovery models, the first was the model established by Rappaport et al. and the second was based on another satellite-derived biomass dataset (Avitabile et al. 2016)[39]. These models were used to estimate the percentage recovery of AGC compared to pre-disturbance (or old-growth) forest values (see Figure 5a of [26]). We compared their estimates to values of relative recovery based on our model of recovery in Amazonian degraded forests (Supplementary Table 20; Supplementary Figure 22). The results based on our recovery model are consistently between the two model results used by Bullock and Woodcock (2021). Given that one of their models is based on field data (G1) and the other on another satellite product (G2), this comparison further supports our model and strengthens the conclusions we can draw from our results.

Comparison with Heinrich et al. (2021)[36]

- Location: Brazilian Amazon biome
- Forest type: Secondary forests
- Data type: Field data (Number of sites: 33)

Heinrich et al. validated their models of secondary forest regrowth across the Brazilian Amazon biome with field data across 33 locations (see Supplementary Table 10 in Heinrich et al)[36]. The same field data were used in this study to compare AGC estimates across various secondary forest age groups (Supplementary Figure 23). Secondary forest and associated median AGC within a 30km radius of the field data were extracted and used for comparison. We also used the secondary forest data based on MapBiomas V3 secondary forest identification and ESA-CCI AGC data in Heinrich et al. (2021) to build a regrowth model for the whole Brazilian Amazon Biome, which was not initially carried out by them[36].

Analysis of the field data shows AGC values in older secondary forests (21 years plus) are not statistically different (p-values between 0.36 and 0.93) and interquartile ranges overlap (Supplementary Figure 23a). In younger secondary forests the AGC values were statistically different ($p < 0.01$), this may be linked to the nature of the definition of secondary forest in the JRC analysis, linked to disturbance rather than regrowth after deforestation specifically. Secondary forests identified in the JRC product may therefore be slightly older than estimated by the product (see Supplementary Note 1 and Supplementary Figure 10a). Further analysis reveals that the effect size is small across the ages (<0.3). We also analysed whether the rate of change between incremental groupings of YSLD were statistically different. The results showed that in both datasets, increments were statistically different between key groups, namely the youngest and oldest secondary forest increments (Supplementary Figure 23b), suggesting that, regardless of the absolute values, the relative change between increments of YSLD was being picked up in both datasets.

The Brazilian Amazon biome regrowth rates based on secondary forest identified with MapBiomas[36] were very similar to the regrowth rates for the whole Amazon region using the secondary forest identified with JRC, and confidence intervals overlap (Supplementary Figure 24). After 20 years of recovery, the AGC (AGC_{20}) was 41.2±2.5 Mg C ha^{-1} and 44.9±2.9 Mg C ha^{-1} for the MapBiomas- and JRC-based secondary forest datasets respectively (Supplementary Figure 24). Although the two models capture slightly different regions, namely the Brazilian Amazon biome and whole Amazon region, the similarity between the two studies is promising. Furthermore, a recent field study showed that estimates provided by Heinrich et al. (2021)[36] of secondary forest regrowth for the eastern Amazon were similar (1.3 Mg C ha^{-1} yr^{-1} [CI_{model}: 1.0 to 1.6]) to the slow regrowth rates estimated by field data in the Brazilian state of Pará (1.23 ± 0.57 Mg C ha^{-1} yr^{-1} [CI_{model}: 0.66 to 1.8])[35], suggesting that wall-to-wall remote sensing data can pick up slower rates of growth.

Supplementary Discussion

Supplementary Discussion 1: Exploring variability and uncertainty in our analysis

In the main part of this paper, we address a few of the uncertainties associated with the analysis. This includes the fact that the space-for-time substitution approach used in this study relied heavily on using sufficient data/pixel points to extract the median value of AGC for a particular forest age/YSLD. Additionally, we address the issue of the spatial resolution which at the scale of 100m for the AGC product may include a mix of undisturbed and disturbed forest, especially at the edges between these pixel classifications. However, we did try to account for this by only extracting forest clusters of the same type above the spatial scale of the AGC product (100m).

Additionally, there are the innate uncertainties and associated errors of the respective data products used, which were discussed to some extent by Heinrich et al[36]. This includes but is not limited to the fact that the L-band signal used to produce the ESA-CCI Aboveground Biomass (AGB) data product saturates at higher AGB/AGC values[40]. This presents a challenge when estimating the AGC of old-growth forest which typically have a higher AGC value but also the older degraded forests which may also have a higher AGC value than represented in the dataset. Partly for this reason, we provide a numerical average growth rate for only the first 20 YSLD.

The space-for-time substitution approach also does not explicitly account for inter-annual variability which may impact growth, such as years of extensive drought or extreme fires. Additionally, it cannot explicitly account for the CO_2 fertilisation effect, which arises with rising atmospheric CO_2 concentrations. However, both these effects are implicitly within the estimates, as the younger forests/ recently degraded forests are growing in an environment with higher CO_2 concentrations than older forests. Additionally, there are more environmental variables that drive recovery beyond the four we explore in this study. For example, soil fertility is known to also influence AGC[21,41] and may be correlated with some of the variables used in this study. However, soil maps available across the pan-tropics currently have high inaccuracies[42] and do not directly capture phosphorous, a key nutrient that influences growth[21].

This analysis provides a holistic, regional analysis of how secondary and degraded forests can recover and regrow by tracking changes in the median AGC values (see methods). Our results do not provide plot specific growth rates which will differ significantly, for example depending on whether the forest is naturally regenerating or actively restored[24].

To account for the spatial variability, we carried out a Monte Carlo simulation analysis (see Methods of main paper). By applying the Monte Carlo simulations, the results show that this remote sensing application can capture significant variability across the regions (Supplementary Figures 14 to 16; Supplementary Table 2). The highest variability, relative to the model fit, is in Borneo, where AGC values varied on average by -12.4 and +11.6 Mg C ha^{-1} in degraded forests. The 95% confidence interval from the Monte Carlo simulations was used throughout this study as the primary measure of variability when referring to the regional models. Incorporating a wall-to-wall analysis, as we have done here, is not possible with field-based chronosequence studies.

However, pixel-based uncertainties of the remote sensing products and model-based uncertainties remain. We combined the standard error of the ESA-CCI dataset with the standard error of the residual (see Methods of main paper). The error propagation shows that most of the uncertainty is associated with the remote sensing product (Supplementary Table 3). The propagated uncertainty was lowest in degraded forests in Borneo (21.5 Mg C ha^{-1}; equal to 31%) and highest in secondary forests in Central Africa (37.1 Mg C ha^{-1}; equal to 78%). We were not surprised by the large propagated standard error of the models. Numerous studies have shown that modelling carbon fluxes associated from the Land-Use Land-Use-Change and Forestry (LULUCF) sector is the most uncertain component of the global carbon budget[43,44], with carbon removals by forests typically having larger uncertainties associated with it than gross emissions[44] due to the complicated nature of forest regrowth. For example, Harris et al. (2021) found that the propagated standard deviation of the removals flux is about 108% in the tropics[44]. This emphasises the ongoing need to quantify the fluxes of the LULUCF and to refine estimates, comparing the estimates and consolidating them. With such large uncertainties, it becomes more important to compare mean/median results to existing field data as we have done in Supplementary Note 2.

Supplementary Figures

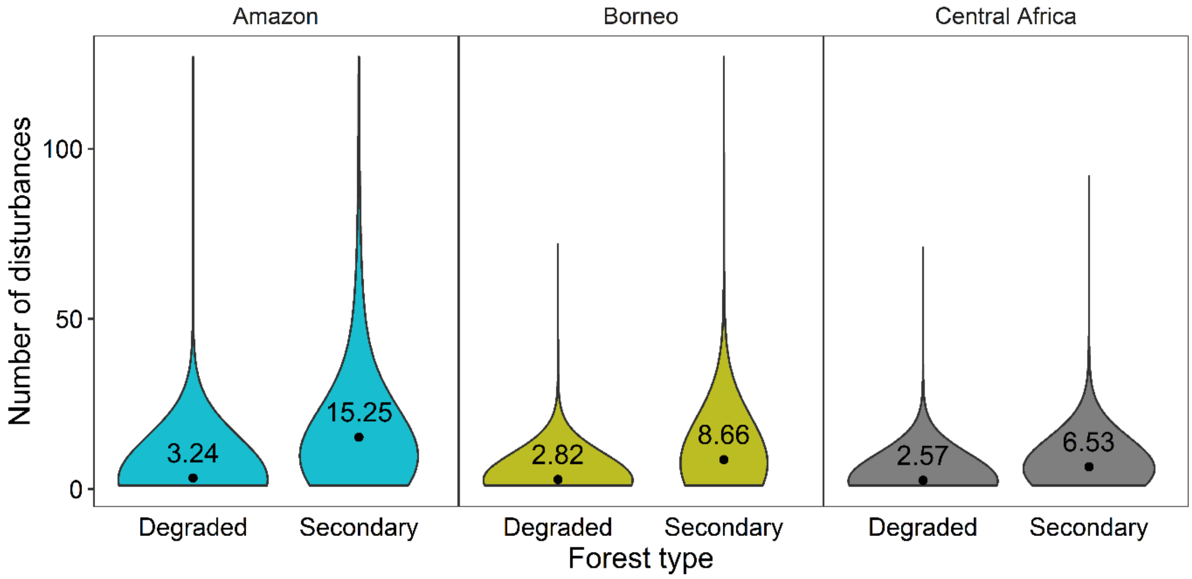

Supplementary Figure 1 | Violin plots of the total number of disturbances experienced by forest clusters in each region and forest type. The violin plots show the range of observed total number of disturbances in connected pixel clusters of degraded and secondary forest over the period 2000 to 2018. This period was selected as it represents the period in which all regions contain enough valid observations. Black dots and associated values represent the mean total number of disturbances across the whole region and forest type.

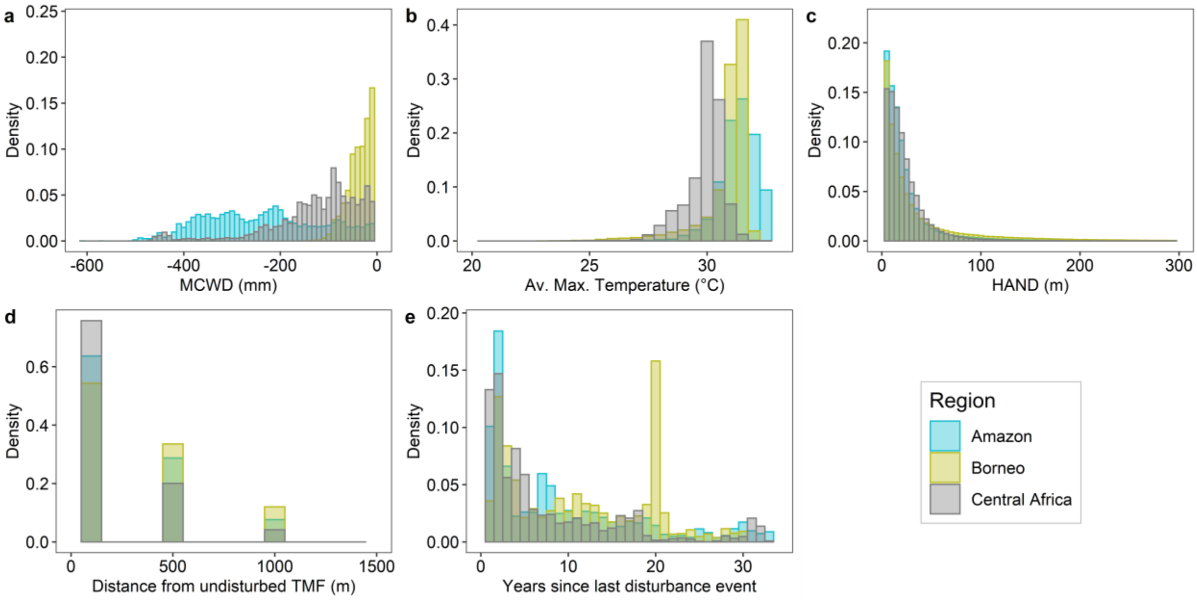

Supplementary Figure 2 | Density distributions of the driving variables in each region and forest type. The variables are (a) Maximum Cumulative Water Deficit; (b) Average Annual Maximum Temperature; (c) Height Above Nearest Drainage (HAND); Distance from nearest undisturbed Tropical Moist Forest (TMF), where the distance of 1000m refers to 1000m plus; and (e) The Years since the last disturbance event (YSLD). The unusually high density of 20 YSLD in Borneo is associated with a period of high disturbance in 1997/1998 associated with a strong El Niño event.

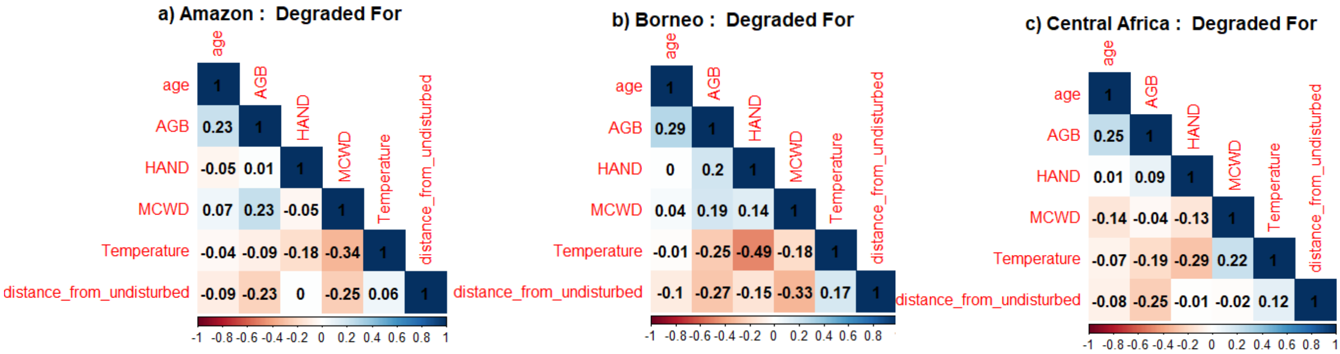

Supplementary Figure 3 | Correlogram showing Pearson's R value between variables in degraded forests. Values show Pearson's R value, and the colouring depicts the relative degree and sign of the relationship between respective variables. If the relationship was non-significant at the 95% confidence interval, no value/shading is shown. Where "age" refers to Years since last disturbance; AGB is Aboveground Biomass; HAND is Height Above Nearest Drainage; MCWD is Maximum Cumulative Water Deficit; Temperature refers to the Average Annual Maximum Temperature; Distance_from_undisturbed is the distance from nearest undisturbed forest.

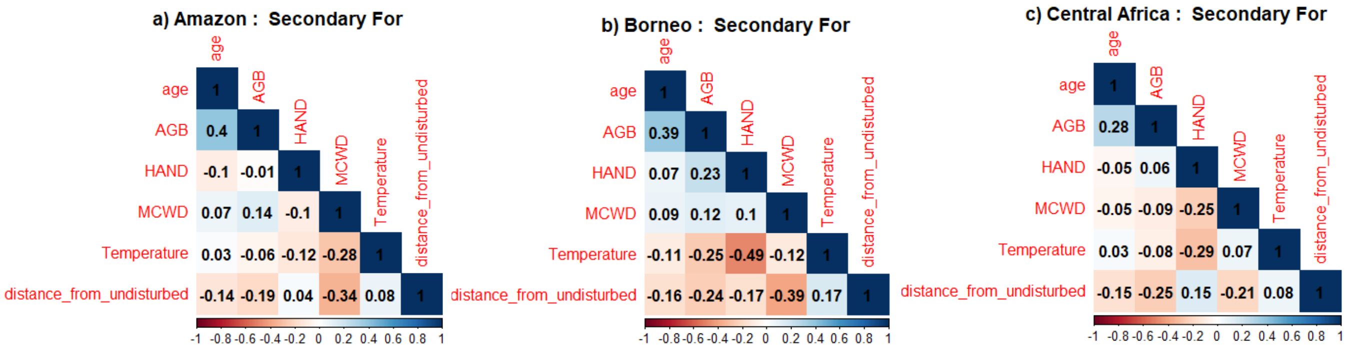

Supplementary Figure 4 | Correlogram showing Pearson's R value between variables in secondary forests. Values show Pearson's R value, and the colouring depicts the relative degree and sign of the relationship between respective variables. If the relationship was non-significant at the 95% confidence interval, no value/shading is shown. Refer to Supplementary Figure 3 for abbreviation definition.

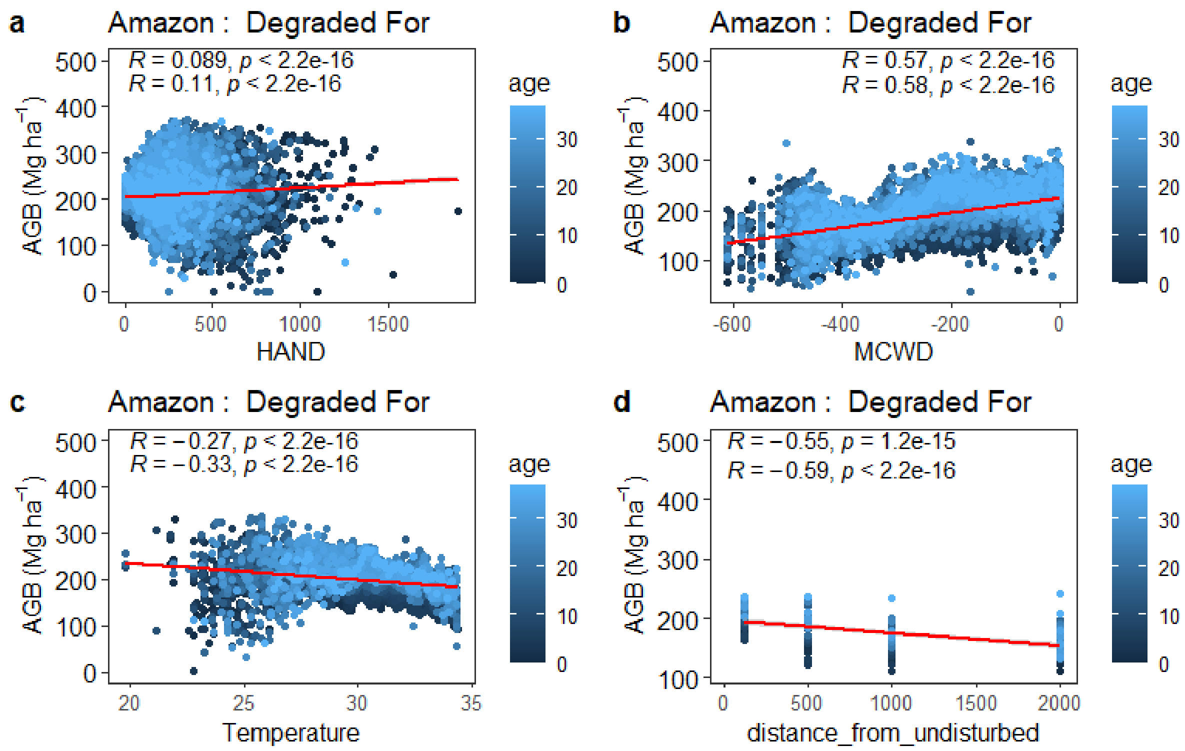

Supplementary Figure 5| Scatterplots of the relationship between driving variables and Aboveground Biomass (AGB) in the Amazon in Degraded Forests. Values show the weighted (by number of pixels) median AGB values detected for each value of the driving variable. R values show Pearson's R (top) and Spearman's Rho (bottom) and the associated p-value. Refer to Supplementary Figure 3 for abbreviation definition. Where "age" refers to the Year Since the Last (forest) Disturbance event.

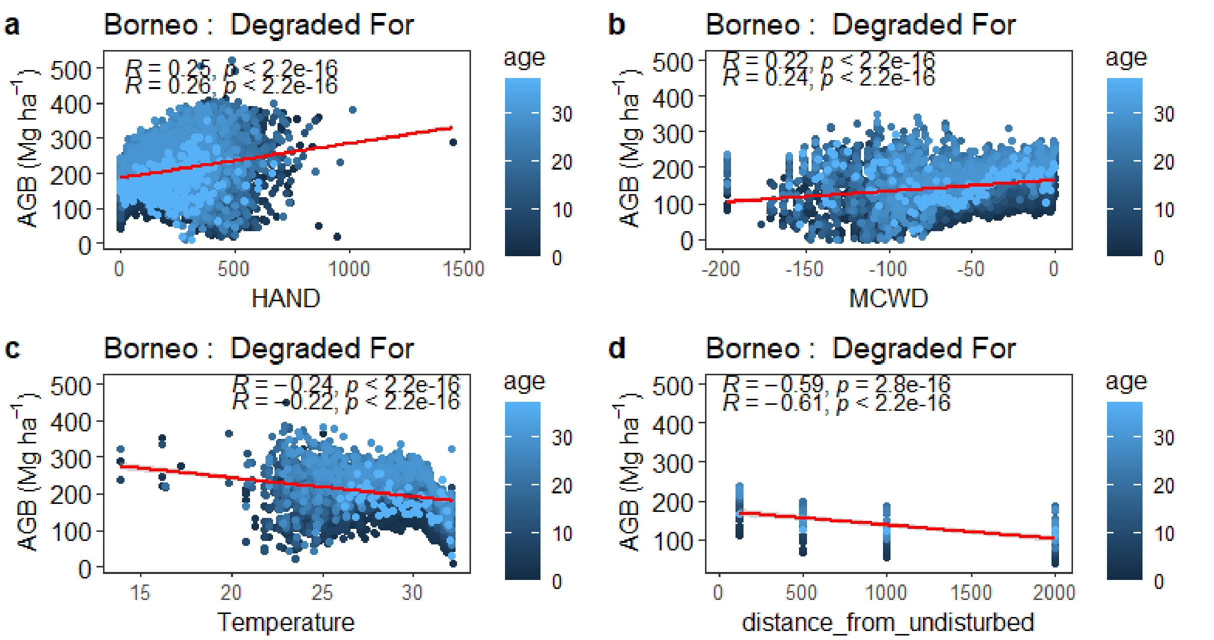

Supplementary Figure 6| Scatterplots of the relationship between driving variables and Aboveground Biomass (AGB) in Borneo in Degraded Forests. Values show the weighted (by number of pixels) median AGB values detected for each value of the driving variable. R values show Pearson's R (top) and Spearman's Rho (bottom) and the associated p-value. Refer to Supplementary Figure 3 for abbreviation definition. Where "age" refers to the Year Since the Last (forest) Disturbance event.

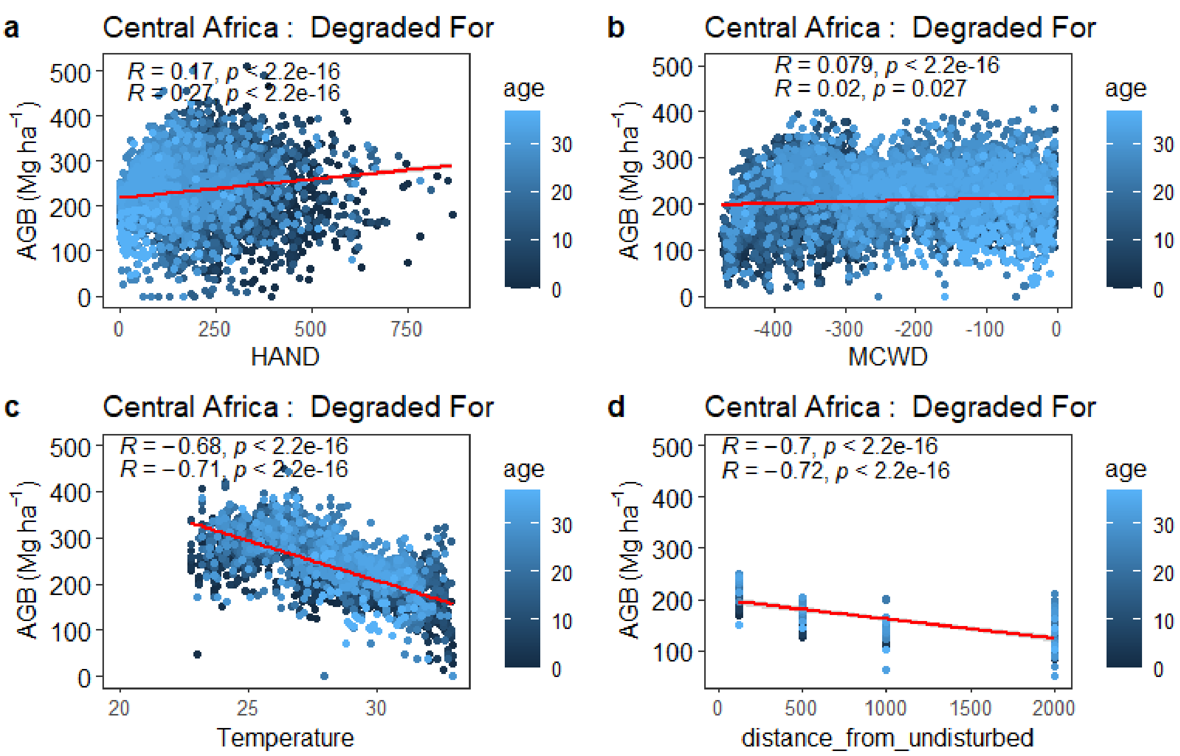

Supplementary Figure 7| Scatterplots of the relationship between driving variables and Aboveground Biomass (AGB) in Central Africa in Degraded Forests. Values show the weighted (by number of pixels) median AGB values detected for each value of the driving variable. R values show Pearson's R (top) and Spearman's Rho (bottom) and the associated p-value. Refer to Supplementary Figure 3 for abbreviation definition. Where "age" refers to the Year Since the Last (forest) Disturbance event.

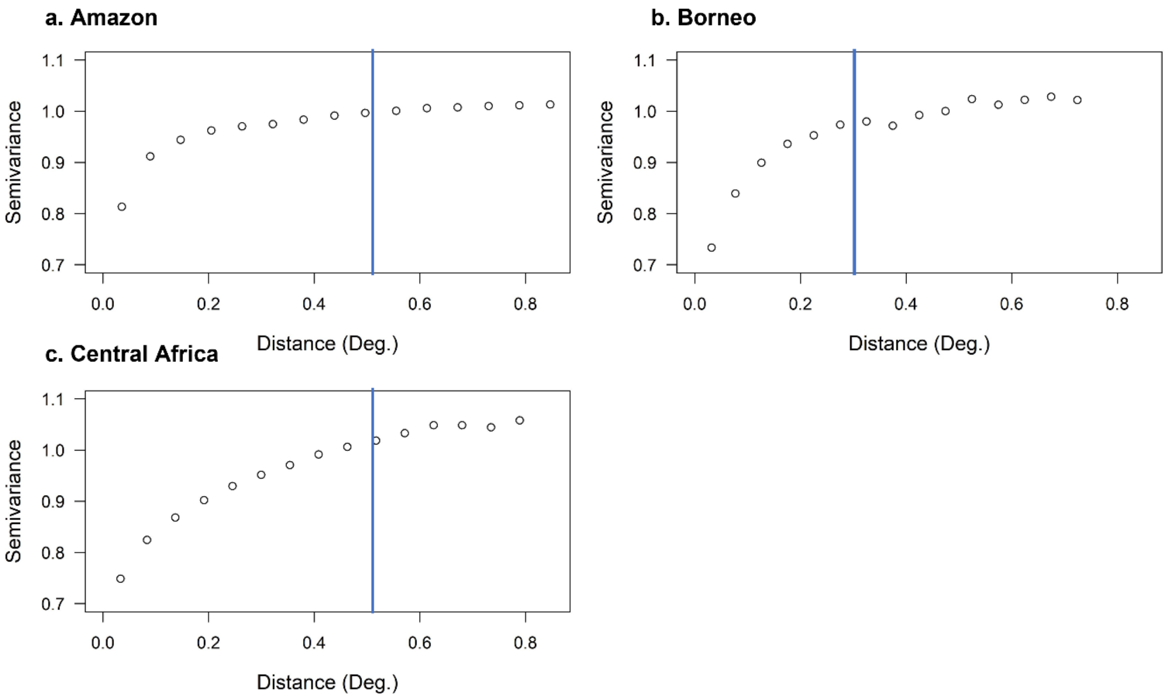

Supplementary Figure 8| Semi-variogram of linear-model residuals across the different regions. Results show the average outputs of numerous semi-variogram model runs within 2x2degree grid squares using degraded forest cells in (a) the Amazon; (b) Borneo; and (c) Central Africa. Blue bars denote the distance (in degrees) at which points the residuals become less spatially-autocorrelated.

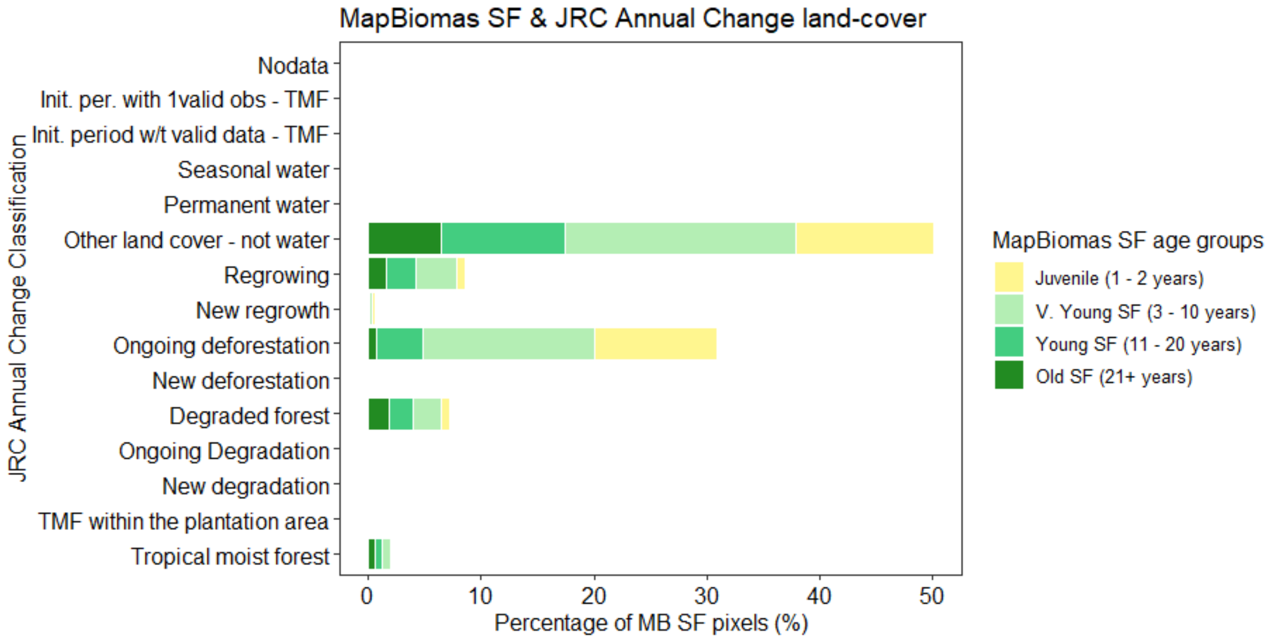

Supplementary Figure 9 | Comparison of pixel classification using the JRC-TMF dataset (this study) and MapBiomas in the Brazilian Amazon in 2018. The percentage of MapBiomas pixels that were classed as secondary forest (SF) and the corresponding pixel classification of the JRC-TMF Annual Change dataset, used in this study.

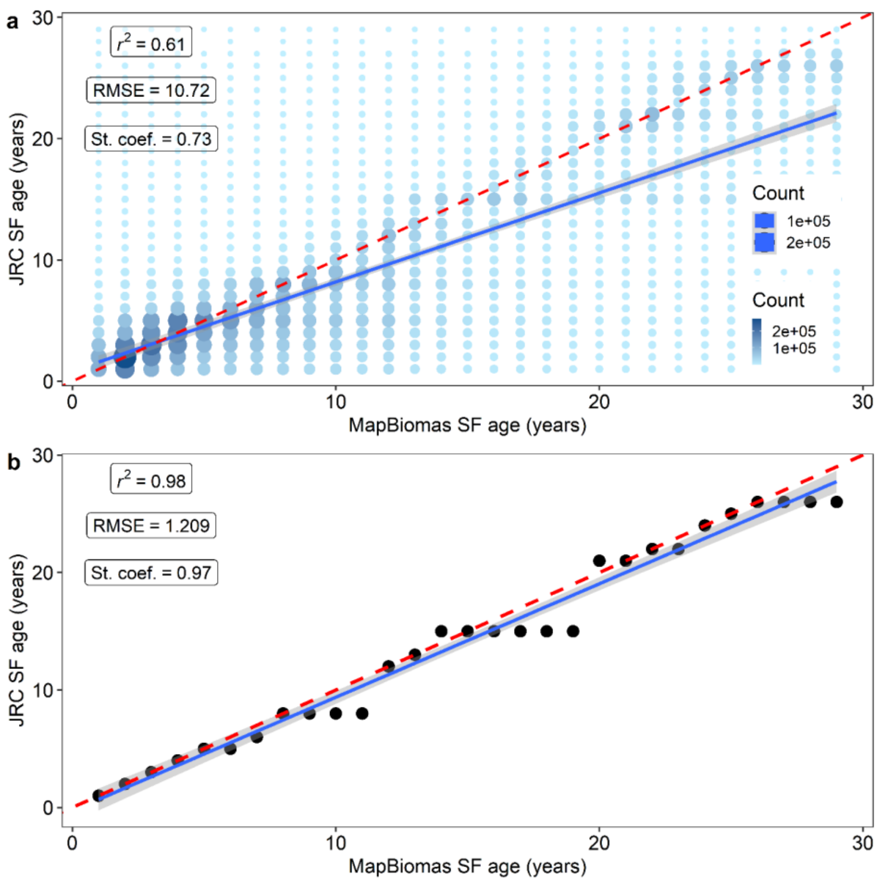

Supplementary Figure 10 | Comparison of the age of secondary forest pixels using the JRC-TMF dataset (this study) and Mapbiomas in the Brazilian Amazon in 2018. The results show (a) a scatter plot weighted by the number of pixels ('count') of the pixel value (age) in the MapBiomas dataset (X-axis) and the JRC-TMF age (Y-axis; this study). (b) the modal value is extracted and plotted, i.e. the corresponding JRC-TMF age with the maximum number of pixels overlapping a certain value (age) of a MapBiomas pixel. Red dotted line shows the corresponding 1:1 expected relationship between the two products. Blue line in each subplot is the modelled linear regression and associated values refer to the coefficient of determination (r^2), the root mean square error (RMSE) and the standardised (beta) coefficient (St. coef.).

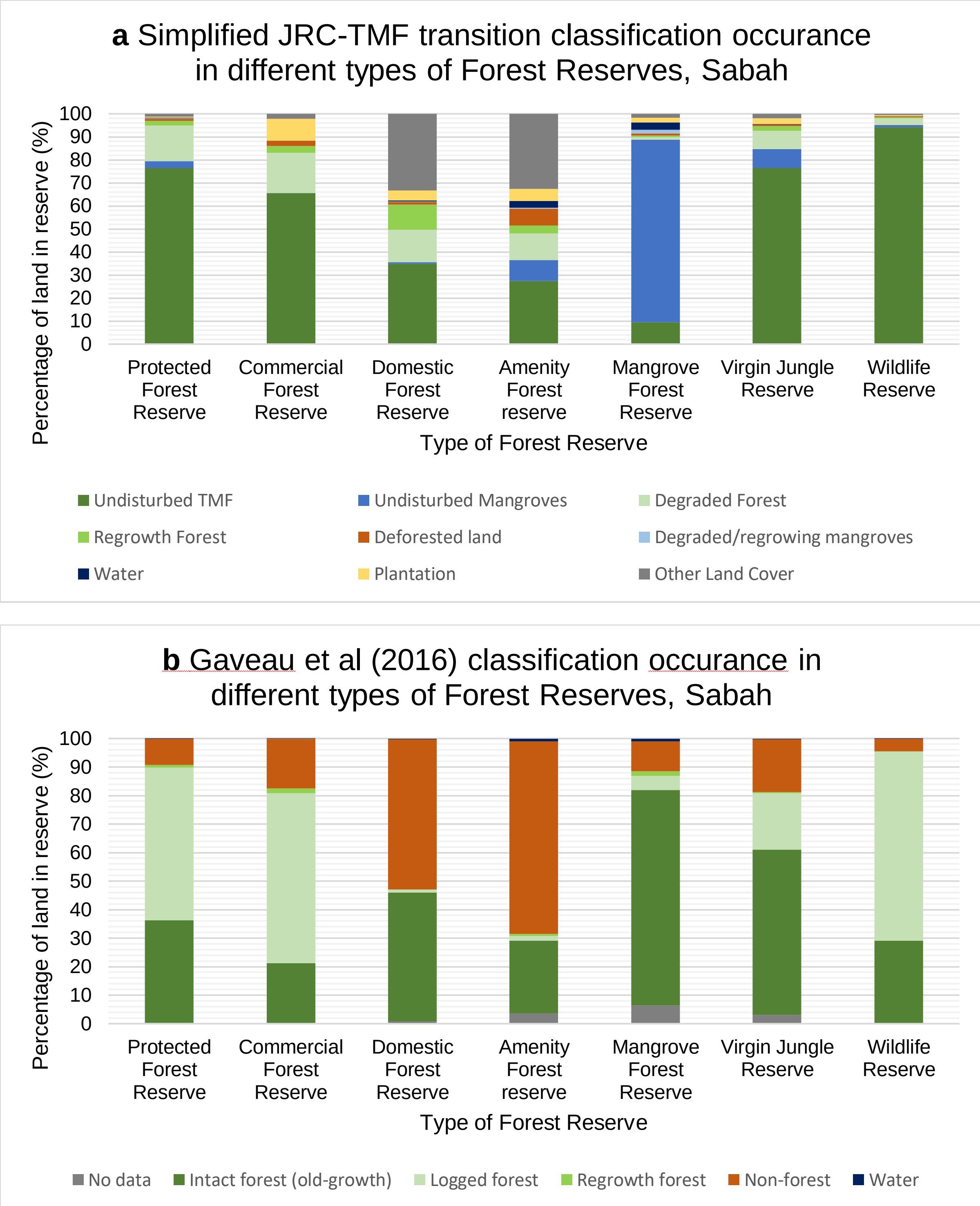

Supplementary Figure 11 | The percentage of land in different types of forest reserves in Sabah, Borneo as classified by different land-cover types. The bar graphs show (a) the forest classification for the year 2019 of the dataset used in this study – JRC-TMF (Vancutsem et al. 2021) and (b) the forest classification for the year 2016 in another study (Gaveau et al. 2016).

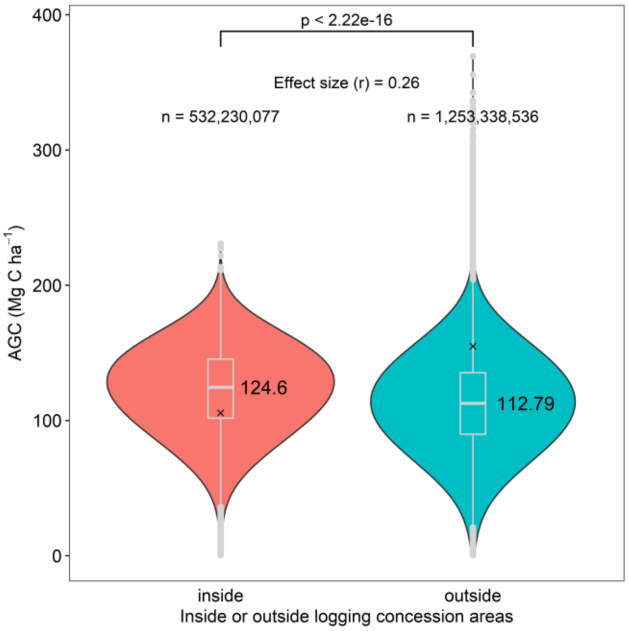

Supplementary Figure 12 | Violin and boxplots showing the distribution of Aboveground Carbon (AGC) inside and outside of logging concession areas of undisturbed forest in Central Africa. Text values denote the median value. The x denotes the weighted-mean AGC value, n is the number of pixels considered in each area. Whether the difference between the two regions is statistical significance was calculated using the Wilcoxon-test and is shown by the p value in the graph. The Wilcoxon effect size provides a measure of the magnitude of the difference between the two groups, where <0.3 is considered a small effect size, 0.3-0.5 is a medium effect size and >0.5 is a large effect size. The difference between the two groups in the figure is therefore quite small.

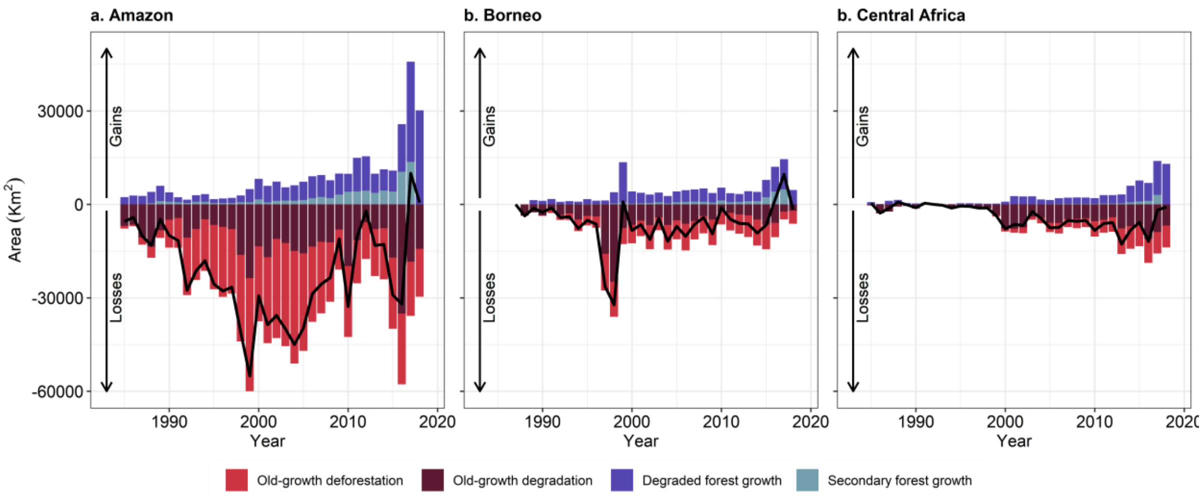

Supplementary Figure 13 | Stacked bar graphs showing the annual forest area gains and losses in different regions across the tropics. Gains include growth of degraded and secondary forests, while losses are considered degradation and deforestation of old-growth forests. Data is shown for the period 1985 to 2018. Black line denotes the annual net change between the gains and the losses. Years with high rates of degradation may precede those with high degraded forest growth.

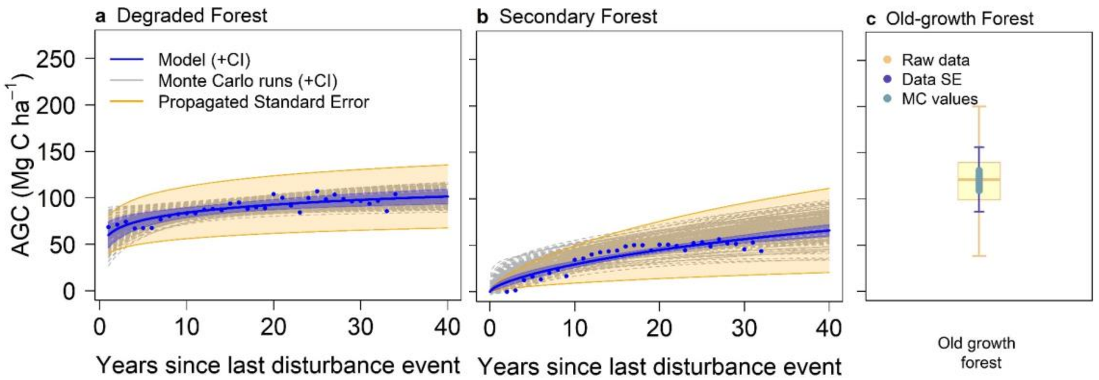

Supplementary Figure 14 | Amazonian regional AGC growth model, its variability and standard error. The graphs show the regional model (reproduced from Figure 1 in main text) and model Confidence Interval (CI) (blue, plus shading), the models based on 50 Monte Carlo (MC) simulations, which used sub-samples of the data (grey lines), and the propagated standard error: combining the residual standard error of the non-linear growth model, with the standard error of the ESA-CCI AGC dataset (yellow, plus shading), in (a) degraded Forests and (b) Secondary Forests. Subplot (c) shows the distribution (as a boxplot) of the raw AGC values of old-growth forests, the standard error of the ESA-CCI data for old-growth forests (purple), and the values used in each MC simulation (grey-blue dots).

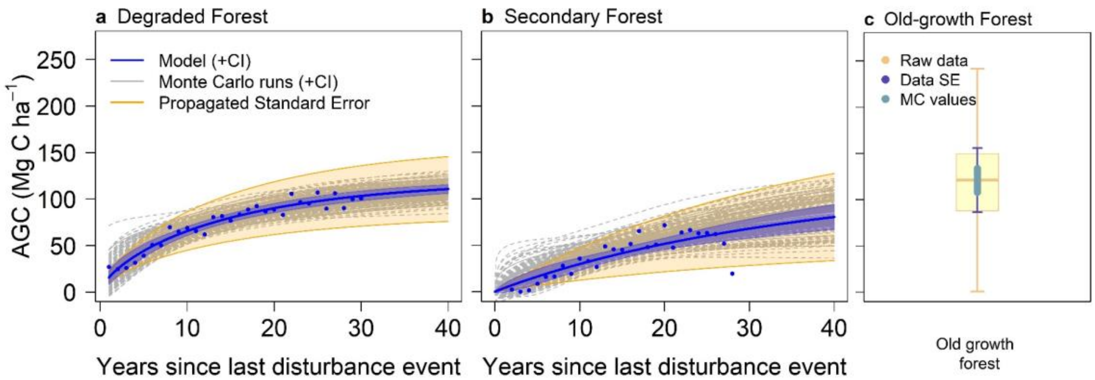

Supplementary Figure 15 | Bornean regional AGC growth model, its variability and standard error. As Supplementary Figure 14 but for forests in Borneo.

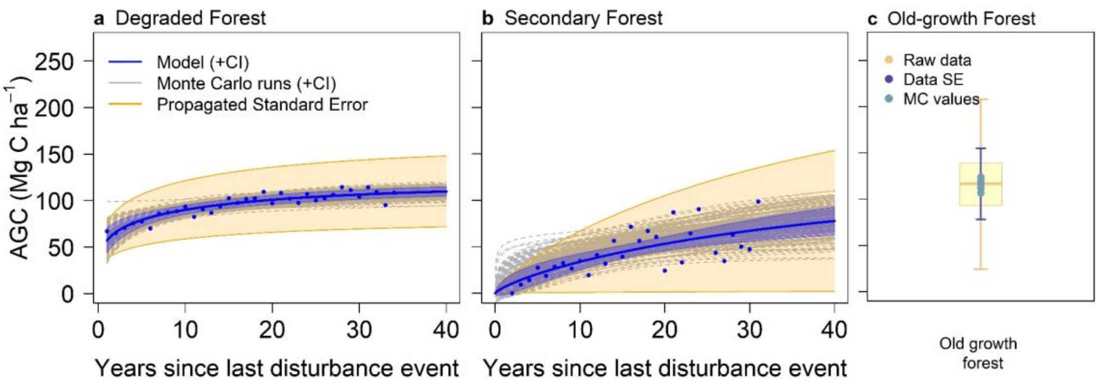

Supplementary Figure 16 | Central African regional AGC growth model, its variability and standard error. As Supplementary Figure 14 but for forests in Central Africa.

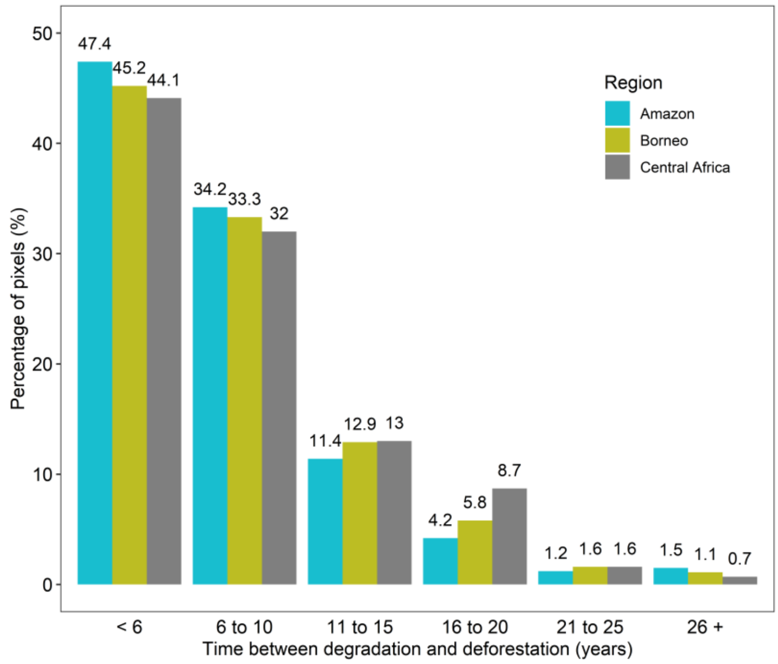

Supplementary Figure 17 | Percentage distribution of the time interval between degradation and deforestation in each region. This graph only includes pixels of degraded forests that were later deforested.

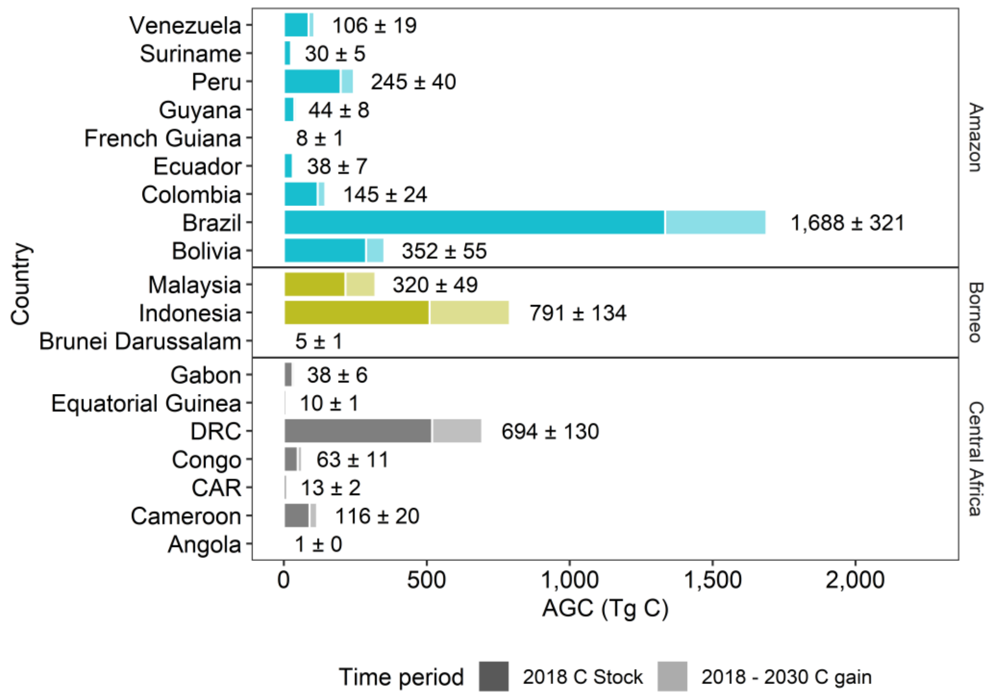

Supplementary Figure 18 | The 2018 carbon (C) stock and maximum technical 2030 carbon sink potential across recovering forests within the three major tropical forest regions grouped by country. Solid bars denote the total carbon accumulated from the beginning of the growth period (since 1984 in the Amazon and Central Africa, and since 1987 in Borneo) to 2018. Lighter bars denote the maximum potential carbon gain from 2018 to 2030 if the 2018 recovering forest area would remain until 2030. The range (±) shows the 95% confidence interval from the Monte Carlo simulations.

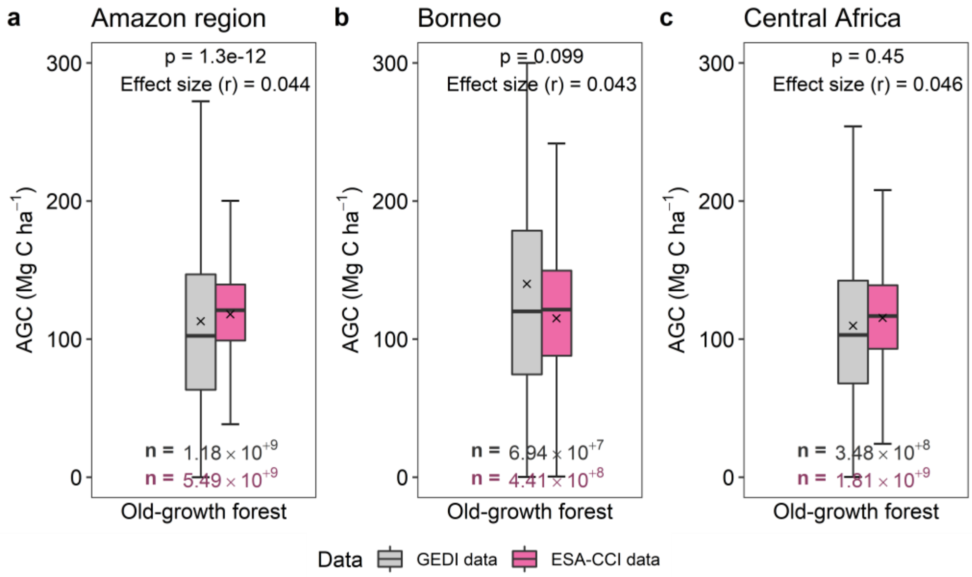

Supplementary Figure 19 | Boxplot comparison of Aboveground Carbon (AGC) estimates obtained from two remote sensing datasets in old-growth forests. Two remote sensing datasets were compared, namely the LiDAR-derived Global Ecosystem Dynamics Investigation (GEDI) and the RADAR-derived ESA-CCI dataset used in this study. The analysis was carried out in the three major tropical regions investigated in this study, (a) the Amazon, (b) Borneo and (c) Central Africa. The X denotes the weighted-mean AGC value, n is the number of pixels considered in each region for each dataset. P-value denotes if the difference between the two datasets is significant or not, based on the non-parametric Wilcox-test. The Wilcoxon effect size provides a measure of the magnitude of the difference between the two groups, where <0.3 is considered a small effect size, 0.3-0.5 is a medium effect size and >0.5 is a large effect size. The difference between the two groups in the figure is very small.

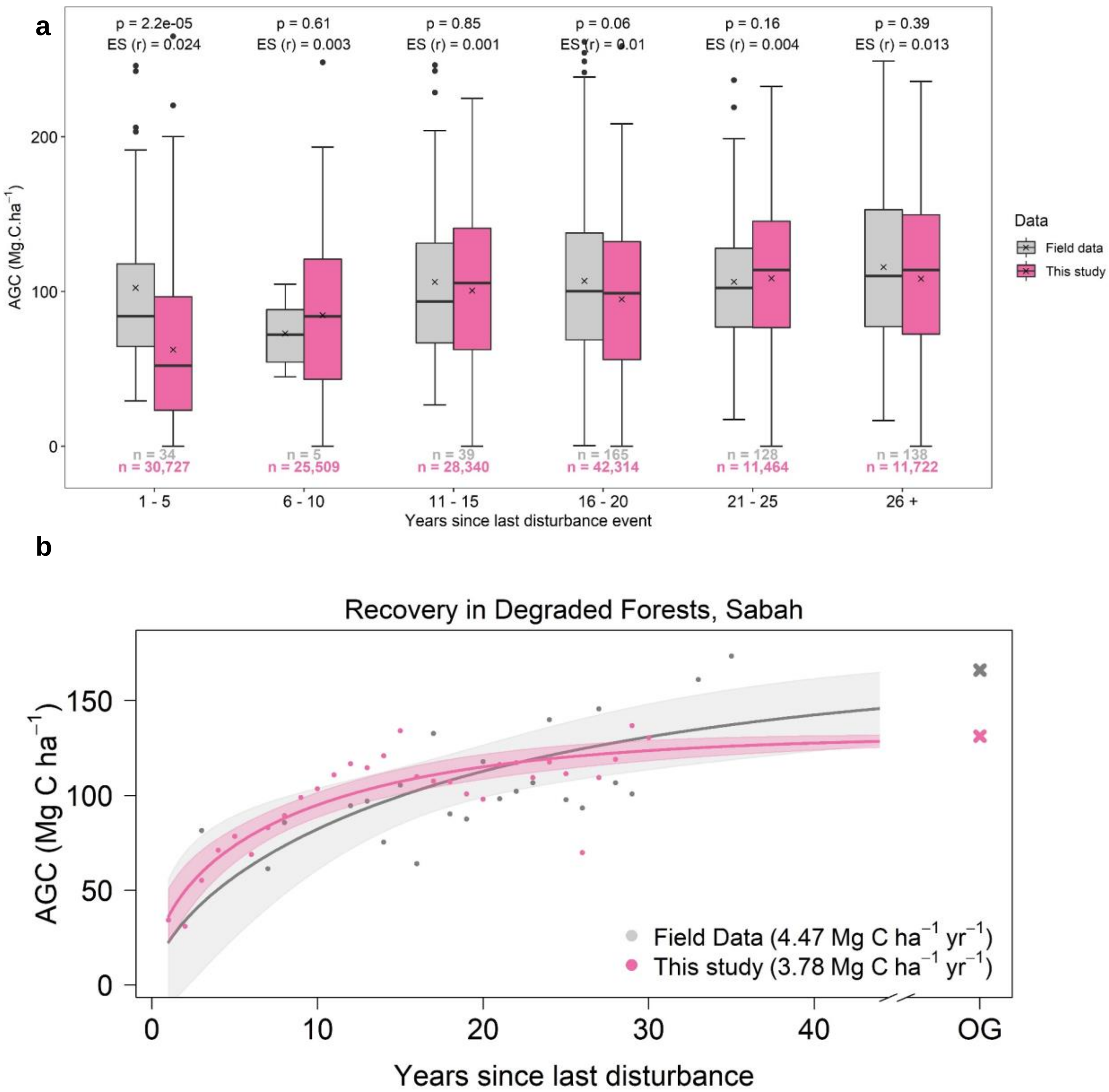

Supplementary Figure 20 | Comparison of degraded forest data and models from this study with field data, Sabah, Malaysian Borneo. (a) The box plots show the Aboveground Carbon (AGC) in degraded forests obtained from field data (Philipson et al. 2020; Cutler et al. 2020) and from the remote sensing data used in this study in the Sabah area only, grouped by different groups of Years since the last disturbance event (YSLD). Boxplots show the interquartile range, the median (straight bar) and the mean values (crosses), n is the number of field measurements and pixels considered for the field data and remote sensing data, respectively. P-value refers to the non-parametric Wilcoxon test to help provide a measure of whether the two datasets are statistically different. The Wilcoxon effect size (ES) provides a measure of the magnitude of the difference between the two groups, where <0.3 is considered a small effect size, 0.3-0.5 is a medium effect size and >0.5 is a large effect size. The difference between the two groups in the figure is therefore very small. (b) the non-linear modelled AGC accumulation with YSLD using the field data and remote sensing data (this study). Dots denote the median AGC value for a specific time, and the corresponding line is the non-linear model. Shaded areas are the 95% confidence interval of the model. Values in the bracket of the legend denote the average AGC accumulation rate in the first 20 years of recovery. Crosses refer to the median old-growth (OG) forest values for the Sabah area from the respective datasets.

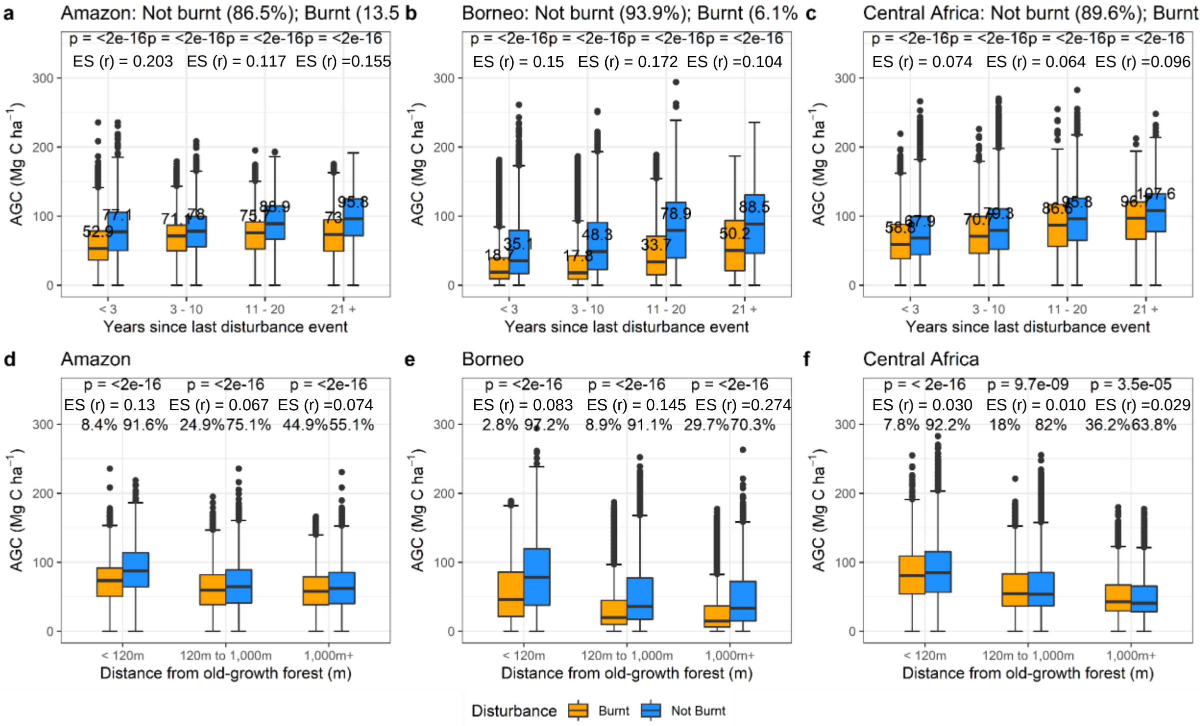

Supplementary Figure 21 | Aboveground carbon (AGC) variation in degraded forests subject to and not subject to burning. Data is shown according to Years since the last disturbance event (a – c) and distance from nearest old-growth forest cluster (d – f). Plots show the median (horizontal line and associated number) AGC values split up according to whether the plots experienced burning (yellow) or not (blue) in (a and d) Amazon; (b and e) Borneo and (c and f) Central Africa. Percentage numbers in brackets (a – c) show the number of clusters subject to burning or not. Percentage numbers within the graphs (d – f) show the proportion of degraded forests subject to burning in that distance category. P-values refer to the non-parametric Wilcoxon test, where p is always <0.01 due to the large size of the dataset used in each region. The Wilcoxon effect size (ES) provides a measure of the magnitude of the difference between the two groups, where <0.3 is considered a small effect size, 0.3-0.5 is a medium effect size and >0.5 is a large effect size.

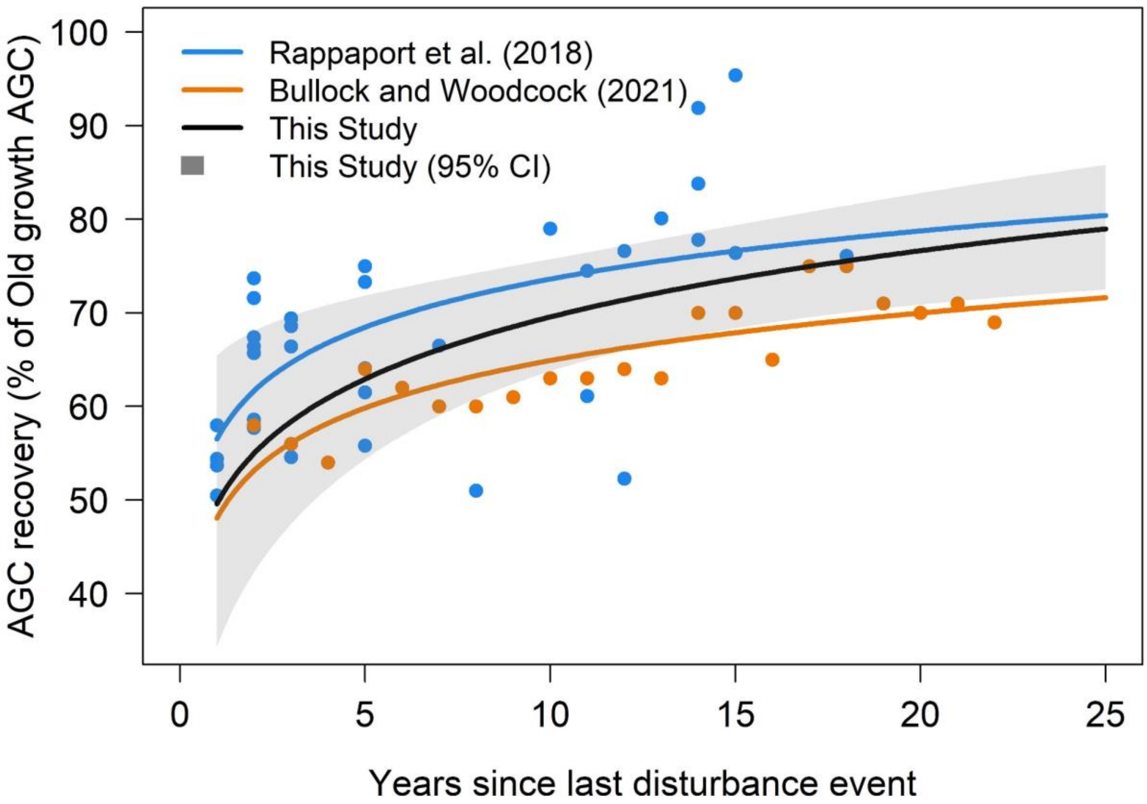

Supplementary Figure 22 | Results from different studies of Aboveground Carbon (AGC) recovery relative to old-growth forest AGC in the Amazon region. Dots denote the average AGC aggregated across the region, which is based on field data in the Mato Grosso region (Rappaport et al. 2018), and remote sensing data (Avitabile et al. 2016) in the whole Amazon region (Bullock and Woodcock, 2021). Lines denote the modelled AGC recovery with time, where curves for Rappaport et al. (2018) and Bullock and Woodcock (2021) are log-based curves, and the curve for out study is a non-linear model (see methods) and the associated 95% confidence interval based on 50 Monte Carlo simulations (see methods).

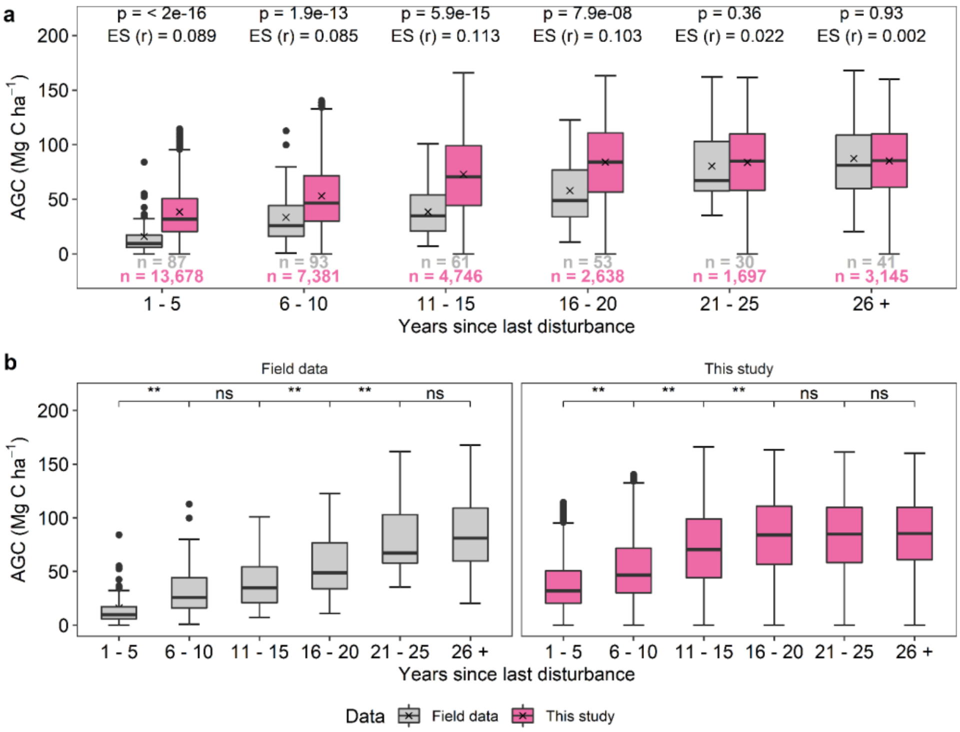

Supplementary Figure 23 | Field data and remote sensing comparison of Secondary Forest Aboveground Carbon (AGC) in the Brazilian Amazon. (a) Directly comparing Secondary Forest AGC grouped by different groups of Years since the last disturbance event (YSLD). Boxplots show the interquartile range, the median (straight bar) and the mean values (crosses). P-values refers to the non-parametric Wilcoxon test to help provide a measure of whether the two datasets are statistically different. (b) Comparing the different groups within the respective datasets to determine whether differences between YSLD groups are statistically different, according to the non-parametric Wilcoxon test. Stars denote if the difference was statistically significant (** : p<0.01) or not (ns). Field data are from several studies and were first collectively introduced in Heinrich et al. (2021)[27].

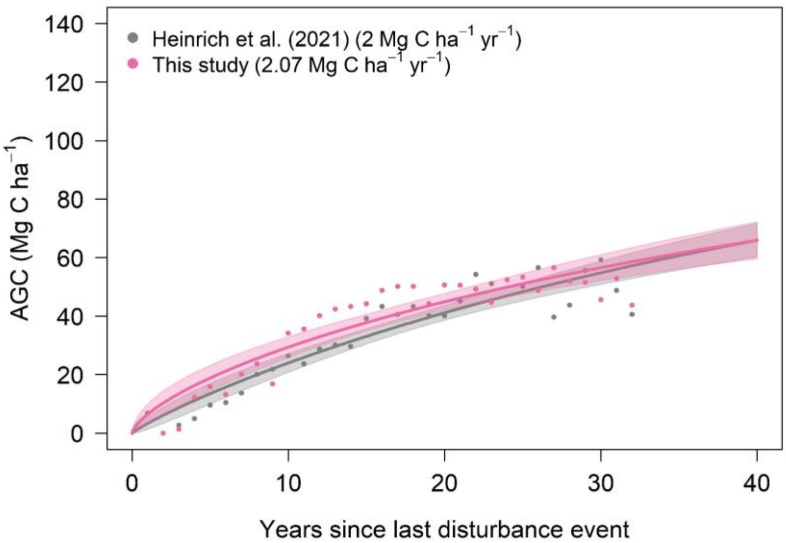

Supplementary Figure 24 | Comparison of Secondary Forest Aboveground Carbon (AGC) regrowth models for the Amazon obtained in this study and a previous one. Points denote the median AGC value calculated for each Year since the last disturbance event (YSLD), fitted lines are based on a non-linear model. Shading denotes the 95% confidence interval of the non-linear model. The two studies are both remote sensing based. Heinrich et al (2021) used MapBiomas to identify ages and extent of secondary forest in the Brazilian Amazon (Grey colours). In this study (pink colours), secondary forest age and extent was estimated using the JRC dataset (Vancutsem et al 2021) and represents the whole Amazon region. Values in the bracket of the legend denote the average AGC accumulation rate in the first 20 years of recovery.

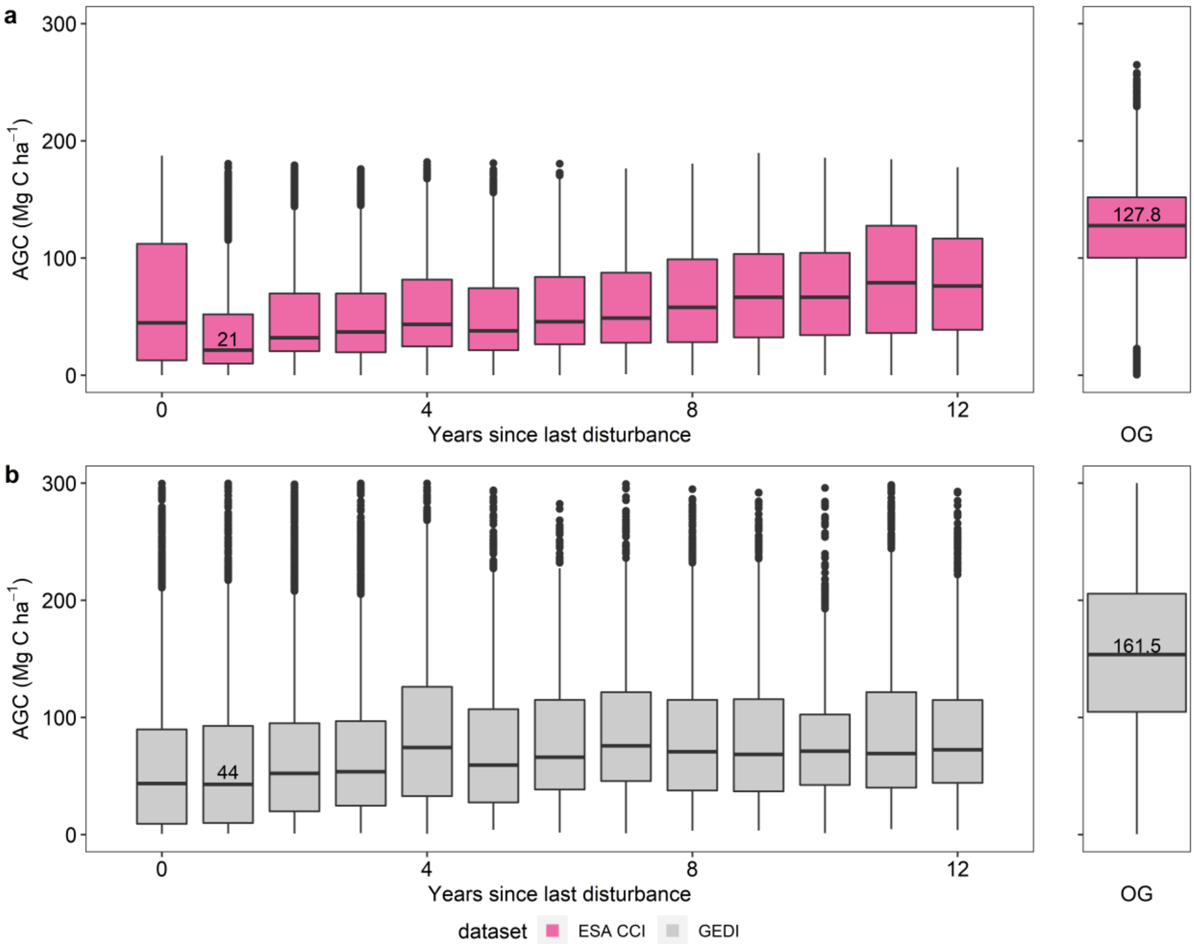

Supplementary Figure 25 | Boxplot comparison of Aboveground Carbon (AGC) estimates obtained from two remote sensing datasets in logging concession areas of East Kalimantan, Borneo. Two remote sensing datasets were compared, (a) the RADAR-derived ESA-CCI dataset used in this study and (b) the LiDAR-derived Global Ecosystem Dynamics Investigation (GEDI) dataset. Boxplots show the range of values for each Year since the last disturbance event as well as old-growth forest values (OG). Thick black lines denote the median value and text represents the median value for 1 YSLD and the old-growth forest value used in the analysis in the text of the Supplementary Material.

Supplementary Tables

Supplementary Table 1 | Primary drivers of forest loss in different regions across the tropics. Data has been extracted from the spatially explicit information from Curtis et al. (2018) and expressed as a percentage (%) below for the relative percentage of the primary driver of forest loss in each $10km^2$ grid square.

	Amazon	Central Africa	Borneo	Brazilian Amazon biome
Commodity driven deforestation	45.7 %	1.4 %	70.1 %	58.4 %
Shifting agriculture	51.9 %	98.0 %	15.2 %	38.9 %
Forestry	1.9 %	0.3 %	14.6 %	2.5 %
Wildfire	0.4 %	0.3 %	0.1 %	0.1 %
Urbanisation	0.0 %	/	/	0.1 %

Supplementary Table 2 | Variability of the non-linear regional growth models. Numbers refer to the average upper and lower limits of the 95% confidence interval (CI) across the years. The Model 95% CI is computed according to the median values used to make the model. The Monte Carlo 95% CI is calculated based on the respective CI of the 50 Monte Carlo simulations based on sub-samples of the data. For absolute differences from model fit, please refer to accompanying data. Note the * of the old-growth forests refers to the absolute minimum and maximum values from the Monte Carlo runs.

Region	Model 95% CI: average difference from model fit in Mg C ha^{-1} (and expressed as a percentage difference from the model fit)	Monte Carlo 95% CI: average difference from model fit expressed as a range (Mg C ha^{-1})
	Degraded Forest	
Amazon	±6.5 (±7.9%)	-9.1 and +9.4
Island of Borneo	±5.3 (±9.9%)	-11.3 and +10.6
Central Africa	±5.7 (±6.6%)	-7.4 and +7.0
	Secondary Forest	
Amazon	±3.6 (11.8%)	-4.7 and +16.3
Island of Borneo	±7.0 (±25.1%)	-11.6 and +21.5
Central Africa	±9.2 (±27.2%)	-11.6 and +19.4
	Old growth Forest	
Amazon	-	-0.7 and +1.7 (*-11.8 and +9.6)
Island of Borneo	-	-1.7 and +1.8 (*-13. 1 and +12.4)
Central Africa	-	-1.0 and +1.0 (*-9.9 and +7.2)

Supplementary Table 3 | Uncertainty (standard error) of the non-linear growth models and aboveground carbon dataset. Numbers refer to the residual standard error as computed by the non-linear model for each region. The standard error of the ESA-CCI dataset is the average of the median standard error estimated for each forest type and Year Since Last Disturbance Event. The propagated standard error combines the error of the model and the dataset using the root square sum method.

Region	Model residual standard error (Mg C ha^{-1})	ESA-CCI data average median standard error (Mg C ha^{-1})	Propagated standard error (Mg C ha^{-1})
Degraded Forest			
Amazon	±14.2 (14.2%)	25.3 (28.8%)	28.9 (33.4%)
Island of Borneo	±10.5 (14.2%)	18.1 (24.9%)	21.5 (31.4%)
Central Africa	±12.4 (11.9%)	29.9 (31.7%)	32.2 (34.7%)
Secondary Forest			
Amazon	±7.1 (17.5%)	23.3 (58.1%)	24.1 (60.7%)
Island of Borneo	±12.7 (28.1%)	13.1 (35.5%)	18.3 (45.3%)
Central Africa	±17.3 (30.9%)	33.1 (71.9%)	37.1 (78.3%)
Old growth Forest			
Amazon	-	34.8 (28.8%)	-
Island of Borneo	-	34.7 (28.6%)	-
Central Africa	-	38.4 (32.9%)	-

Supplementary Table 4 | Key inputs and outputs from the growth model analysis by region shown in Figure 1 of the paper. Old-growth forest Aboveground carbon (AGC) values refer to A in equation 1 of the main paper. Final column shows the 95% confidence interval of the model (CI_{model}) as well as from the Monte Carlo simulations as was shown in the main text (CI_{MC}).

Region	Old-growth forest AGC (AGC at 1 YSLD) (Mg C ha^{-1})	RMSE (Mg C ha^{-1})	Est. time of Asymptote (years)	<20 yr Avg. growth rate as Mg C ha^{-1} yr^{-1} (top) and % increase per year (bottom)	Model 95% CI (top) and Monte Carlo 95% CI (bottom) (Mg C ha^{-1} yr^{-1}) in first 20 years of growth
Degraded Forest growth					
Amazon	121 (60)	13.7	163	1.49 1.4%	±0.14 ±0.17
Island of Borneo	121 (16)	10.2	86	3.60 3.2%	±0.45 ±0.87
Central Africa	117 (57)	12.0	84	1.98 2.0%	±0.16 ±0.19
Secondary Forest growth					
Amazon	121	6.8	243	2.07 1.7%	±0.32 ±0.83
Island of Borneo	121	12.2	159	2.52 2.1%	±0.94 ±1.21
Central Africa	117	16.7	243	2.51 2.1%	±1.02 ±1.19

Supplementary Table 5 | Summary statistics from the non-linear models of forest recovery in each region shown in Figure 1 of the main paper. Values of k and c are the key coefficients determined by the model and reflect the growth rate and shape of the growth curve respectively. The associated standard error, t-values and p-values are shown for k and c. Stars are a visually accessible way of assessing whether the statistics is significant, where: p <0.001 ('***'); p < 0.01 ('**'); p < 0.05('*'); p < 0.1 ('.'); p < 1.0 (' ')

Region	Values of k and c in (1) to 3d.p	Standard Error of k and c	t-value of k and c	Pr(>|t|) of k and c	Degrees of freedom
Degraded Forest growth					
Amazon	0.009 0.150	0.006 0.045	1.43 3.29	0.16 0.002 **	33
Island of Borneo	0.053 0.685	0.009 0.109	6.03 6.27	1.5e-06 *** 7.7e-07 ***	29
Central Africa	0.036 0.212	0.013 0.54	2.75 3.95	0.01 *** 0.0004 ***	33
Secondary Forest growth					
Amazon	0.013 0.671	0.003 0.095	4.03 7.03	0.0004 *** 9.77e-08 ***	29
Island of Borneo	0.026 0.959	0.027 0.959	0.01 0.25	0.006 ** 0.0007 ***	25
Central Africa	0.022 0.768	0.010 0.250	2.21 3.07	0.036 * 0.0048 **	27

Supplementary Table 6 | Results from a Kruskal-Wallis analysis testing the statistically significant difference between region growth curves. The model results were compared and assessed at the 95% confidence interval to determine whether the difference between the models was statistically significantly different. Ticks (crosses) denote that the models are (not) statistically significantly different. Values outside the brackets denote the outputs for the degraded forest models, values in brackets are the outputs for the secondary forest models.

	Amazon	Island of Borneo	Central Africa
Amazon		✓ (✓)	✓ (✓)
Island of Borneo	✓ (✓)		× (×)
Central Africa	✓ (✓)	× (×)	

Supplementary Table 7 | key inputs and outputs from the growth model analysis by Average Maximum Annual Temperature (Tmax) shown in Figure 2 of the paper.

Region	Old-growth forest AGC (Mg C ha^{-1})	RMSE (Mg C ha^{-1})	Est. time of Asymptote (years)	Values of k and c in (1) to 3d.p	<20 yr Avg. growth rate (Mg C $ha^{-1} yr^{-1}$) plus Model 95% CI	AGC after 20 years of recovery (Mg C ha^{-1})
Degraded Forest growth						
Amazon						
19.8 to 30.8°C	112	16.7	83	0.031/0.159	1.56 (±0.17)	99 ±6.9
30.9 to 31.8°C	117	14.2	138	0.014/0.168	1.61 (±0.16)	92 ±5.7
31.9 to 34.4°C	101	12.8	84	0.025/0.133	1.23 (±0.11)	89 ±5.3
Island of Borneo						
13.9 to 30.6°C	119.5	19.3	34	0.168/0.731	3.85 (±0.70)	117 ±5.8
30.7 to 31.3°C	119.5	9.2	77	0.064/0.855	3.9 (±0.50)	90±4.6
31.4 to 32.2°C	76	8.4	47	0.118/1.325	3.07 (±0.67)	67 ±4.2
Central Africa						
22.8 to 29.6°C	123	16.7	76	0.038/0.164	1.76 (±0.17)	111 ±7.0
29.7 to 30.3°C	114	12.7	85	0.036/0.231	2.05 (±0.18)	98 ±5.4
30.4 to 33.0°C	114	12.7	94	0.030/0.215	1.93 (±0.17)	96 ±5.3
Secondary Forest growth						
Amazon						
19.8 to 30.9°C	112	9.9	180	0.019/0.689	2.37 (±0.47)	51 ±3.8
31.0 to 31.9°C	117	9.7	233	0.014/0.666	2.06 (±0.45)	45 ±3.7
32.0 to 34.4°C	101	9.7	241	0.011/0.595	1.73 (±0.41)	39 ±3.7
Island of Borneo						
21.8 to 30.9°C	120	13.4	105	0.046/1.065	3.44 (±1.00)	70 ±6.5
31.0 to 31.4°C	112	10.5	125	0.038/1.206	2.60 (±0.89)	52 ±4.9
31.5 to 32.2°C	72	11.7	90	0.052/1.342	2.00 (±1.19)	39 ±5.7
Central Africa						
22.8 to 29.8	123	22.7	186	0.020/0.770	2.47 (±1.34)	52 ±10.1
29.9 to 30.3°C	113	18.1	176	0.020/0.706	2.43 (±0.96)	52 ±7.8
30.4 to 32.2°C	114	23.0	154	0.022/0.520	2.79 (±0.93)	67 ±9.8

Supplementary Table 8 | Results from a Kruskal-Wallis analysis testing the statistically significant difference of growth curves within regions in different regions of Average Annual Maximum Temperature. The model results were compared and assessed at the 95% confidence interval to determine whether the difference between the models was statistically significantly different. Ticks (crosses) denote that the models are (not) statistically significantly different. Values outside the brackets denote the outputs for the degraded forest models, values in brackets are the outputs for the secondary forest models.

Average Annual Maximum Temperature (°C)			
Amazon			
	Lowest 25%	**Middle 50%**	**Upper 25%**
Lowest 25%		✓ (✓)	× (✓)
Middle 50%	✓ (×)		✓ (✓)
Upper 25%	× (✓)	✓ (×)	
Island of Borneo			
	Lowest 25%	**Middle 50%**	**Upper 25%**
Lowest 25%		✓ (✓)	✓ (✓)
Middle 50%	✓ (✓)		✓ (✓)
Upper 25%	✓ (✓)	✓ (✓)	
Central Africa			
	Lowest 25%	**Middle 50%**	**Upper 25%**
Lowest 25%		× (×)	✓ (✓)
Middle 50%	× (×)		✓ (×)
Upper 25%	✓ (✓)	✓ (×)	

Supplementary Table 9 | Key inputs and outputs from the growth model analysis by Maximum Cumulative Water Deficit (MCWD) shown in Extended Data Figure 3 of the paper.

Region	Old-growth forest AGC (Mg C ha^{-1})	RMSE (Mg C ha^{-1})	Est. time of Asymptote (years)	Values of k and c in (1) to 3d.p	<20 yr Avg. growth rate (Mg C ha^{-1} yr^{-1}) plus Model 95% CI	AGC after 20 years of recovery (Mg C ha^{-1})
Degraded Forest growth						
Amazon						
-611 to -323 mm	86	9.9	53	0.046/0.127	0.99 (±0.08)	80 ±4.1
-322 to -138 mm	124	16.0	156	0.011/0.161	1.62 (±0.17)	96 ±6.4
-137 to 0 mm	127	16.0	120	0.019/0.168	1.79 (±0.17)	105 ±6.6
Island of Borneo						
-197 to -44 mm	104	11.8	102	0.041/0.717	2.85 (±0.57)	68 ±5.7
-43 to -6 mm	119	9.1	87	0.054/0.791	3.63 (±0.47)	86 ±4.5
-5 to 0 mm	122	15.7	52	0.103/0.776	4.23 (±0.71)	110 ±7.2
Central Africa						
-474 to -161 mm	119	14.1	97	0.023/0.146	1.57 (±0.14)	102 ±5.8
-160 to -61 mm	115	13.2	80	0.039/0.225	2.04 (±0.18)	100 ±5.6
-60 to -4 mm	110	16.5	60	0.060/0.255	2.12 (±0.20)	100 ±7.3
Secondary Forest growth						
Amazon						
-611 to -352 mm	85	6.2	185	0.016/0.646	1.68 (±0.30)	36 ±2.6
-351 to -159 mm	120	7.2	240	0.013/0.679	2.07 (±0.36)	45 ±3.0
-158 to 0 mm	128	13.3	208	0.017/0.672	2.50 (±0.69)	55 ±5.7
Island of Borneo						
-197 to -62 mm	100	14.0	105	0.044/0.096	2.76 (±1.3)	56 ±7.8
-61 to -17 mm	117	15.3	128	0.024/0.991	2.23 (±1.3)	46 ±7.8
-16 to 0 mm	124.5	12.3	133	0.034/0.961	3.06 (±0.9)	63 ±6.4
Central Africa						
-471 to -188 mm	123	16.1	300	0.006/0.425	1.89 (±0.67)	47 ±7.8
-187 to -79 mm	114	19.1	129	0.036/1.167	2.63 (±1.87)	53±9.8
-78 to -4 mm	110	15.6	142	0.028/0.833	2.63 (±1.19)	55 ±10.9

Supplementary Table 10 | Results from a Kruskal-Wallis analysis testing the statistically significant difference of growth curves within regions in different regions of MCWD. The model results were compared and assessed at the 95% confidence interval to determine whether the difference between the models was statistically significantly different. Ticks (crosses) denote that the models are (not) statistically significantly different. Values outside the brackets denote the outputs for the degraded forest models, values in brackets are the outputs for the secondary forest models.

Maximum Cumulative Water Deficit; MCWD (mm yr^{-1})			
Amazon			
	Lowest 25%	**Middle 50%**	**Upper 25%**
Lowest 25%		✓ (✓)	✓ (✓)
Middle 50%	✓ (✓)		✓ (×)
Upper 25%	✓ (✓)	✓ (×)	
Island of Borneo			
	Lowest 25%	**Middle 50%**	**Upper 25%**
Lowest 25%		✓ (✓)	✓ (✓)
Middle 50%	✓ (✓)		✓ (✓)
Upper 25%	✓ (✓)	✓ (✓)	
Central Africa			
	Lowest 25%	**Middle 50%**	**Upper 25%**
Lowest 25%		✓ (×)	✓ (✓)
Middle 50%	✓ (×)		✓ (✓)
Upper 25%	✓ (✓)	✓ (✓)	

Supplementary Table 11 | Key inputs and outputs from the growth model analysis by Height Above Nearest Drainage (HAND) shown in Extended Data Figure 4 of the paper.

Region	Old-growth forest AGC (Mg C ha^{-1})	RMSE (Mg C ha^{-1})	Est. time of Asymptote (years)	Values of k and c in (1) to 3d.p	<20 yr Avg. growth rate (Mg C ha^{-1} yr^{-1}) plus Model 95% CI	AGC after 20 years of recovery (Mg C ha^{-1})
Degraded Forest growth						
Amazon						
1 to 6m	118	14.7	158	0.008/0.126	1.30 (±0.13)	93 ±5.8
7 to 24m	121	13.5	180	0.008/0.150	1.46 (±0.15)	90 ±54
25 to 1902m	108	13.0	79	0.035/0.187	1.69 (±0.16)	95 ±5.5
Island of Borneo						
1 to 6m	121	9.3	111	0.041/0.913	3.26 (±0.57)	72 ±4.5
7 to 39m	122	8.7	103	0.042/0.686	3.37 (±0.39)	83 ±4.2
40 to 1455m	124	16.7	72	0.060/0.455	3.31 (±0.47)	105 ±7.9
Central Africa						
1 to 7m	117	14.4	113	0.021/0.180	1.73 (±0.16)	96 ±5.9
8 to 27m	117	12.3	98	0.028/0.214	1.97 (±0.16)	98 ±5.1
28 to 886m	118	13.2	71	0.044/0.195	1.91 (±0.16)	100 ±7.3
Secondary Forest growth						
Amazon						
1 to 6m	119	7.8	231	0.014/0.669	2.10 (±0.39)	46 ±3.3
7 to 26m	122	5.9	248	0.013/0.671	2.04 (±0.30)	45 ±2.5
27 to 1165m	108	8.2	232	0.013/0.617	1.92 (±0.39)	47 ±3.5
Island of Borneo						
1 to 2m	121	11.0	187	0.022/1.056	2.02 (±1.17)	41 ±5.8
3 to 23m	120	12.0	172	0.024/0.994	2.26 (±0.97)	46 ±6.1
24 to 1186m	124.5	12.0	125	0.037/1.018	3.16 (±0.94)	65 ±6.2
Central Africa						
1 to 10m	116	15.8	166	0.023/0.819	2.48 (±1.05)	52 ±8.0
11 to 32m	117	15.8	154	0.027/0.900	2.57 (±1.13)	53 ±7.6
33 to 542m	115	21.6	253	0.009/0.438	2.12 (±0.85)	54 ±9.8

Supplementary Table 12 | Results from a Kruskal-Wallis analysis testing the statistically significant difference of growth curves within regions in different regions of Height Above Nearest Drainage (HAND). The model results were compared and assessed at the 95% confidence interval to determine whether the difference between the models was statistically significantly different. Ticks (crosses) denote that the models are (not) statistically significantly different. Values outside the brackets denote the outputs for the degraded forest models, values in brackets are the outputs for the secondary forest models.

Height Above Nearest Drainage; HAND (m)			
Amazon			
	Lowest 25%	**Middle 50%**	**Upper 25%**
Lowest 25%		× (×)	✓ (×)
Middle 50%	× (×)		✓ (×)
Upper 25%	✓ (×)	✓ (×)	
Island of Borneo			
	Lowest 25%	**Middle 50%**	**Upper 25%**
Lowest 25%		× (✓)	✓ (✓)
Middle 50%	× (✓)		✓ (✓)
Upper 25%	✓ (✓)	✓ (✓)	
Central Africa			
	Lowest 25%	**Middle 50%**	**Upper 25%**
Lowest 25%		✓ (×)	✓ (✓)
Middle 50%	✓ (×)		✓ (✓)
Upper 25%	✓ (✓)	✓ (✓)	

Supplementary Table 13 | Key inputs and outputs from the growth model analysis by Distance from nearest Old-growth forest shown in Extended Data Figure 5 of the paper.

Region	Old-growth forest AGC (Mg C ha^{-1})	RMSE (Mg C ha^{-1})	Est. time of Asymptote (years)	Values of k and c in (1) to 3d.p	<20 yr Avg. growth rate (Mg C ha^{-1} yr^{-1}) plus Model 95% CI	AGC after 20 years of recovery (Mg C ha^{-1})
Degraded Forest growth						
Amazon						
< 120m	121	15.4	152	0.009/0.126	1.34 (±0.14)	96 ±6.2
120m to 1000m	121	12.3	200	0.008/0.184	1.61 (±0.16)	84 ±4.9
1000m +	121	10.0	172	0.001/0.090	0.78 (±0.32)	73 ±3.9
Island of Borneo						
< 120m	121	15.0	70	0.066/0.593	3.64 (±0.55)	101 ±7.2
120m to 1000m	121	12.2	208	0.014/0.453	2.22 (±0.38)	63 ±5.6
1000m +	121	13.2	299	0.008/0.462	1.77 (±0.44)	49 ±5.9
Central Africa						
< 120m	117	13.2	74	0.039/0.176	1.75 (±0.15)	105 ±5.7
120m to 1000m	117	11.6	223	0.006/0.186	1.49 (±0.16)	77 ±4.6
1000m +	117	15.5	166	0.001/0.111	0.69 (±1.62)	55 ±6.1
Secondary Forest growth						
Amazon						
< 120m	121	7.9	272	0.011/0.648	1.91 (±0.39)	42 ±3.4
120m to 1000m	121	19.9	235	0.014/0.713	2.06 (±1.14)	45 ± 8.4
1000m +	121	8.2	300	0.005/0.516	1.57 (±0.36)	36 ±3.6
Island of Borneo						
< 120m	121	11.0	132	0.034/1.052	2.87 (±0.89)	57 ±5.7
120m to 1000m	121	14.2	235	0.015/0.788	1.95 (±0.94)	41 ±7.1
1000m +	121	13.1	172	0.024/1.026	2.26 (±1.14)	46 ±7.1
Central Africa						
< 120m	117	17.6	212	0.016/0.672	2.21 (±0.98)	48 ±8.3
120m to 1000m	117	23.7	150	0.028/0.893	2.63 (±1.81)	55 ±10.9
1000m +	117	24.6	246	0.011/0.522	2.13 (±1.28)	50 ±14.2

Supplementary Table 14 | Results from a Kruskal-Wallis analysis testing the statistically significant difference of growth curves within regions in different distances from nearest Old-growth forest. The model results were compared and assessed at the 95% confidence interval to determine whether the difference between the models was statistically significantly different. Ticks (crosses) denote that the models are (not) statistically significantly different. Values outside the brackets denote the outputs for the degraded forest models, values in brackets are the outputs for the secondary forest models.

Distance from nearest Old-growth forest (m)			
Amazon			
	< 120m	**120m to 1000m**	**1000m +**
< 120m		✓ (×)	✓ (×)
120m to 1000m	✓ (×)		✓ (✓)
1000m +	✓ (×)	✓ (✓)	
Island of Borneo			
	< 120m	**120m to 1000m**	**1000m +**
< 120m		✓ (✓)	✓ (✓)
120m to 1000m	✓ (✓)		✓ (✓)
1000m +	✓ (✓)	✓ (✓)	
Central Africa			
	< 120m	**120m to 1000m**	**1000m +**
< 120m		✓ (✓)	✓ (×)
120m to 1000m	✓ (✓)		✓ (✓)
1000m +	✓ (×)	✓ (✓)	

Supplementary Table 15 | The total number of connected pixel clusters in each forest type and each region used to build the models. Each cluster of pixels was identified using the tool "Region Group" available in ArcGIS Pro and filtered to remove smaller clusters, where the number of pixels was less than 9. The numbers shown are the number of clusters that were greater than an area of approximately 900m^2 (see methods).

	Amazon	Island of Borneo	Central Africa
Degraded Forest	3,665,707	2,161,795	1,490,616
Secondary Forest	940,475	404,473	54,970

Supplementary Table 16 | Inter-study comparison of the area, carbon stock and AGC of secondary forests in the Brazilian Amazon. Each column refers to a different study conducted in the Brazilian Amazon using various types of remote sensing data to identify secondary forest and their carbon stock and carbon density. Values have been converted to reflect the AGB to AGC conversion factor used in this study (0.456).

	This study –JRC-TMF	**This study – MapBiomas**	**Heinrich et al. 2020[36]**	**Nunes et al. 2020[8]**	**Silva Junior et al. 2020[10]**	**Smith et al. 2020[9]**
Study year	2018	2018	2017	2017	2018	2017
Area (Mha)	5.0	16.9	13.8	12.0	14.9	12.9
Carbon Stock (Tg C)	119 ± 22	470.5	268.1 ±46	299 (Above and below)	388± 25	320 ± 49
Average AGC Mg C ha^{-1}	23.7	27.8	19.4	24.9	26.1	24.8
Secondary forest definition	Years since last disturbance event	Years since last "anthropic" to forest transition	Years since last "anthropic" to forest transition	Years since last "anthropic" to forest transition	Years since last "anthropic" to forest transition	Years since last "anthropic" to forest transition. With a minimum 0.36ha area
Carbon Equation applied	Growth rates calculated by region and age	Growth rates calculated by region and age	Growth rates calculated based on climate and human impact	Growth rates based on previous field study	Growth rate for whole neo-tropics	Growth rates based on ecozones and age
Dataset used	JRC-TMF	MapBiomas V5	MapBiomas V3.1	MapBiomas V3.1	MapBiomas V4.1	MapBiomas V3.1

Supplementary Table 17 | The main functions, packages and software used in the study

Step in method	**Functions (package)**	**Software**
Preparing and processing TMF dataset	Multiple	Google Earth Engine
Group connected forest pixels into clusters	Region Group	ArcPy (Python 3.6.10) ArcPy
Extract large forest clusters	Extract By Attribute	ArcPy (Python 3.6.10)
Determine the modal AGC value for a given forest cluster	Zonal Statistics as Table	ArcPy (Python 3.6.10)
Determine modal value of environmental variable for given forest cluster	Zonal Statistics as Table	ArcPy (Python 3.6.10)
Widen perimeter of old-growth forest	Expand	ArcPy (Python 3.6.10)
Apply Chapman-Richard model for growth	nls (nlstools)[45]	R (v4.0.2)
Determine spatial autocorrelation	variogram, vgm (gstat)[46,47]	R (v4.0.2)
Multi-linear model assessment	corrplot (corrplot) scale (base) lm (lme4)	R (v4.0.2)

Supplementary Table 18 | Aboveground carbon (AGC) regrowth of secondary forest expressed as the percentage recovery relative to old-growth forest AGC in the Amazon across this and previous studies. The primary comparison was to Poorter et al. (2021). Values are based on Figure 2 of Poorter et al. (2021)[31]. Value in bracket refers specifically to field plot data in the Amazon region, extracted using data provided by the published study. Values from Cook-Patton et al. (2020)[32] use the mean growth rate for the Amazon region (4.7 Mg C ha^{-1} yr^{-1}) as well as the minimum and maximum value (2.4 Mg C ha^{-1} yr^{-1}, 5.6 Mg C ha^{-1} yr^{-1}), assuming a linear relationship over the first 30 years of growth. The old-growth forest value was determined using the mean refined IPCC 2019 update value for old-growth forests in the Americas (see Table 1 of Rozendaal et al. (2022)[34] (140 Mg C ha^{-1}). The range in brackets for our study is the lower and upper 95% confidence interval values from the Monte Carlo simulations.

AGB/AGC recovery time	Poorter et al. (2021) Neotropics (Amazon only)	Cook-Patton et al. (2020)	This study – Amazon secondary forests
After 20 years	33% (34%)	66% (min: 35%; max: 81%)	37% (36% to 49%)
After 30 years	45%	99% (min: 52%; max: 121%)	47% (42% to 60%)
After 100 years	85%	-	81% (63% to 97%)
After 120 years	90%	-	85% (67% to 100%)

Supplementary Table 19 | Aboveground carbon (AGC) regrowth of degraded forest expressed as the percentage recovery relative to old-growth forest AGC in the Amazon in this and a previous study (Rappaport et al., 2018). Values in brackets refer to the lower and upper Confidence Intervals (CI), where the CI in our study is based on the Monte Carlo (MC) simulations, expressed as a percentage (%). Recovery is split up according to disturbance type in Rappaport et al (2018), namely logging and burned (once). In our study we do not make this distinction.

	Rappaport et al. (2018) (Lower to Upper CI)		This study – Amazon degraded forests (Lower to Upper MC CI)
Recovery time	**Logged (% of Old-growth Forest)**	**Burned x1 (% of Old-growth Forest)**	**Degraded forest (% of Old-growth Forest)**
After 1 Year	54.8% (49.4 to 60.3)	45.8% (38.0 to 53.6)	49.6% (34.3 to 65.2)
After 5 Years	71.0% (67.5 to 74.5)	61.9% (56.3 to 67.6)	62.9% (54.2 to 71.7)
After 10 Years	77.9% (73.6 to 82.3)	68.9% (63.1 to 74.7)	69.6% (63.6 to 75.6)
After 15 Years	82.0% (76.9 to 87.1)	73.0% (66.8 to 79.1)	73.7% (68.2 to 79.1)

Supplementary Table 20 | Aboveground carbon (AGC) regrowth of degraded forest expressed as the percentage recovery relative to old-growth forest AGC in the Amazon in this and a previous study (Bullock and Woodcock, 2021). Relative recovery estimates are based on two models in Bullock and Woodcock (2021) – G1 which are based on collated results from Rappaport et al., (2018) and G2 – which are based on satellite data used in Bullock and Woodcock (2021) and another remote sensing AGC product - the Avitabile et al., 2016 dataset.

	Bullock and Woodcock (2021)		This study – Amazon degraded forests (Lower to Upper MC CI)
Recovery time	**G1 (Rappaport et al., 2018 model)**	**G2 (Bullock and Woodcock, 2021 model based on satellite data)**	**Degraded forest (% of Old-growth Forest)**
After 1 Year	56.5%	48.1%	49.6% (34.3 to 65.2)
After 5 Years	68.5%	59.8%	62.9% (54.2 to 71.7)
After 10 Years	73.6%	64.9%	69.6% (63.6 to 75.6)
After 15 Years	76.6%	67.9%	73.7% (68.2 to 79.1)
After 20 Years	78.8%	70.0%	76.5% (70.7 – 82.6)

References

1. Qie, L. *et al.* Erratum: Author Correction: Long-term carbon sink in Borneo's forests halted by drought and vulnerable to edges (Nature communications (2017) 8 1 (1966)). *Nat. Commun.* **9**, 342 (2018).

2. Hubau, W. *et al.* Asynchronous carbon sink saturation in African and Amazonian tropical forests. *Nature* **579**, 80–87 (2020).

3. Gatti, L. V. *et al.* Amazonia as a carbon source linked to deforestation and climate change. *Nature* **595**, (2021).

4. Vancutsem, C. *et al.* Long-term (1990–2019) monitoring of forest cover changes in the humid tropics. *Sci. Adv.* **7**, eabe1603 (2021).

5. Santoro, M. & Cartus, O. ESA Biomass Climate Change Initiative (Biomass_cci): Global datasets of forest above-ground biomass for the years 2010, 2017 and 2018, v2. *Centre for Environmental Data Analysis* http://dx.doi.org/10.5285/84403d09cef3485883158f4df2989b0c (2021) doi:10.5285/84403d09cef3485883158f4df2989b0c.

6. Mapbiomas Brasil. Project MapBiomas - Collection 5.0 of Brazilian Land Cover and Use Map Series. https://mapbiomas.org/ (2020).

7. Souza, C. M. *et al.* Reconstructing three decades of land use and land cover changes in brazilian biomes with landsat archive and earth engine. *Remote Sens.* **12**, (2020).

8. Nunes, S., Jr. Oliveira, L., Siqueira, J., Morton, D. C. & Souza, C. M. Unmasking secondary vegetation dynamics in the Brazilian Amazon. *Environ. Res. Lett.* **15**, (2020).

9. Smith, C. C. *et al.* Secondary forests offset less than 10% of deforestation-mediated carbon emissions in the Brazilian Amazon. *Glob. Chang. Biol.* 1–15 (2020) doi:10.1111/gcb.15352.

10. Silva Junior, C. H. L. *et al.* Benchmark maps of 33 years of secondary forest age for Brazil. *Sci. Data* **7**, 269 (2020).

11. Requena Suarez, D. *et al.* Estimating aboveground net biomass change for tropical and subtropical forests: Refinement of IPCC default rates using forest plot data. *Glob. Chang. Biol.* **25**, 3609–3624 (2019).

12. Gaveau, D. L. A. *et al.* Rapid conversions and avoided deforestation: Examining four decades of industrial plantation expansion in Borneo. *Sci. Rep.* **6**, 1–13 (2016).

13. Global Forest Watch. Managed Forest concessions. www.globalforestwatch.org (2020).

14. Jucker, T. *et al.* Estimating aboveground carbon density and its uncertainty in Borneo's structurally complex tropical forests using airborne laser scanning. *Biogeosciences* **15**, 3811–3830 (2018).

15. Poulsen, J. R. *et al.* Old growth Afrotropical forests critical for maintaining forest carbon. *Glob. Ecol. Biogeogr.* **29**, 1785–1798 (2020).

16. Ferraz, A. *et al.* Carbon storage potential in degraded forests of Kalimantan, Indonesia. *Environ. Res. Lett.* **13**, (2018).

17. Dubayah, R. *et al.* The Global Ecosystem Dynamics Investigation: High-resolution laser ranging of the Earth's forests and topography. *Sci. Remote Sens.* **1**, (2020).

18. Duncanson, L. *et al.* Biomass estimation from simulated GEDI, ICESat-2 and NISAR across environmental gradients in Sonoma County, California. *Remote Sens. Environ.* **242**, 111779 (2020).

19. GEDI. Dataset: Global Ecosystem Dynamics Investigation (GEDI). https://daac.ornl.gov/cgi-bin/dataset_lister.pl?p=40? (2022).

20. Cuni-Sanchez, A. *et al.* High aboveground carbon stock of African tropical montane forests. *Nature* **596**, 536–542 (2021).

21. Lewis, S. L. *et al.* Above-ground biomass and structure of 260 African tropical forests. *Philos. Trans. R. Soc. B Biol. Sci.* **368**, (2013).

22. Labrière, N. *et al.* Toward a forest biomass reference measurement system for remote sensing applications. *Glob. Chang. Biol.* 1–14 (2022) doi:10.1111/gcb.16497.

23. Duncanson, L. *et al.* Global AGB Maps Inter-comparison exercise using Plot2Map tool [Gabon]. https://repo.ops.maap-project.org/lduncanson/biomass_harmonization/-/blob/master/plot2map_50GabonVal_1km.ipynb (2022).

24. Philipson, C. D. *et al.* Active restoration accelerates the carbon recovery of human-modified tropical forests. *Science (80-.).* **369**, 838–841 (2020).

25. Rappaport, D. I. *et al.* Quantifying long-term changes in carbon stocks and forest structure from Amazon forest degradation. *Environ. Res. Lett.* **13**, (2018).

26. Bullock, E. L. & Woodcock, C. E. Carbon loss and removal due to forest disturbance and regeneration in the Amazon. *Sci. Total Environ.* **764**, 142839 (2021).

27. Avitabile, V. *et al.* An integrated pan-tropical biomass map using multiple reference datasets. *Glob. Chang. Biol.* **22**, 1406–1420 (2016).

28. Cutler, M. E. J. *et al.* Aboveground carbon density plots from a logged forest, Danum Valley, Borneo, 1992-2016 (Dataset). *NERC Environmental Information Data Centre.* (2020) doi:https://doi.org/10.5285/a75e6371-a931-4676-9199-d1f5af565ab2.

29. Griscom, B., Ellis, P. & Putz, F. E. Carbon emissions performance of commercial logging in East Kalimantan, Indonesia. *Glob. Chang. Biol.* **20**, 923–937 (2014).

30. Asner, G. P. *et al.* Mapped aboveground carbon stocks to advance forest conservation and recovery in Malaysian Borneo. *Biol. Conserv.* **217**, 289–310 (2018).

31. Poorter, L. *et al.* Multidimensional tropical forest recovery. *Science (80-.).* **374**, 1–8 (2021).

32. Cook-Patton, S. C. *et al.* Mapping carbon accumulation potential from global natural forest regrowth. *Nature* **585**, 545–550 (2020).

33. Craven, D. Multi Dimensional Recovery. *Zenodo* (2021) doi:https://doi.org/10.5281/zenodo.4993023.

34. Rozendaal, D. *et al.* Aboveground forest biomass varies across continents, ecological zones and successional stages: refined IPCC default values for tropical and subtropical forests. *Environ. Res. Lett.* **17**, 014047 (2022).

35. Elias, F. *et al.* Comparing contemporary and lifetime rates of carbon accumulation from secondary forests in the eastern Amazon. *For. Ecol. Manage.* **508**, 120053 (2022).

36. Heinrich, V. H. A. *et al.* Large carbon sink potential of secondary forests in the Brazilian Amazon to mitigate climate change. *Nat. Commun.* **12**, 1785 (2021).

37. Rutishauser, E. *et al.* Rapid tree carbon stock recovery in managed Amazonian forests. *Curr. Biol.* **25**, R787–R788 (2015).

38. Didan, K. MOD13Q1 MODIS/Terra Vegetation Indices 16-Day L3 Global 250m SIN Grid V006. NASA EOSDIS Land Processes DAAC. http://doi.org/10.5067/MODIS/MOD13Q1.006. *USGS* vol. 5 2002–2015 (2015).

39. Avitabile, V. *et al.* An integrated pan-tropical biomass map using multiple reference datasets. *Glob. Chang. Biol.* **22**, 1406–1420 (2016).

40. Santoro, M. & Cartus, O. ESA Biomass Climate Change Initiative (Biomass_cci): Global datasets of forest above-ground biomass for the year 2017, v1. Centre for Environmental Data Analysis. *2019* https://catalogue.ceda.ac.uk/uuid/bedc59f37c9545c981a839eb552e4084 (2019).

41. Moran, E. F. *et al.* Effects of soil fertility and land-use on forest succession in Amazônia. *For. Ecol. Manage.* **139**, 93–108 (2000).

42. Moulatlet, G. M. *et al.* Using digital soil maps to infer edaphic affinities of plant species in Amazonia: Problems and prospects. *Ecol. Evol.* **7**, 8463–8477 (2017).

43. Friedlingstein, P. *et al.* Global Carbon Budget 2020. *Earth Syst. Sci. Data* **12**, 3269–3340 (2020).

44. Harris, N. L. *et al.* Global maps of twenty-first century forest carbon fluxes. *Nat. Clim. Chang.* **11**, 234–240 (2021).

45. Baty, F. nlstools (1.0-2). https://rdocumentation.org/packages/nlstools/versions/1.0-2 (2015).

46. Pebesma, E. J. Multivariable geostatistics in S: The gstat package. *Comput. Geosci.* **30**, 683–691 (2004).

47. Pebesma, E. gstat: Spatial and Spatio-Temporal Geostatistical Modelling, Prediction and Simulation. https://github.com/r-spatial/gstat/ (2021).